iScience

CellPress
OPEN ACCESS

Article

20S proteasome enhancers prevent cytotoxic tubulin polymerization-promoting protein induced α-synuclein aggregation

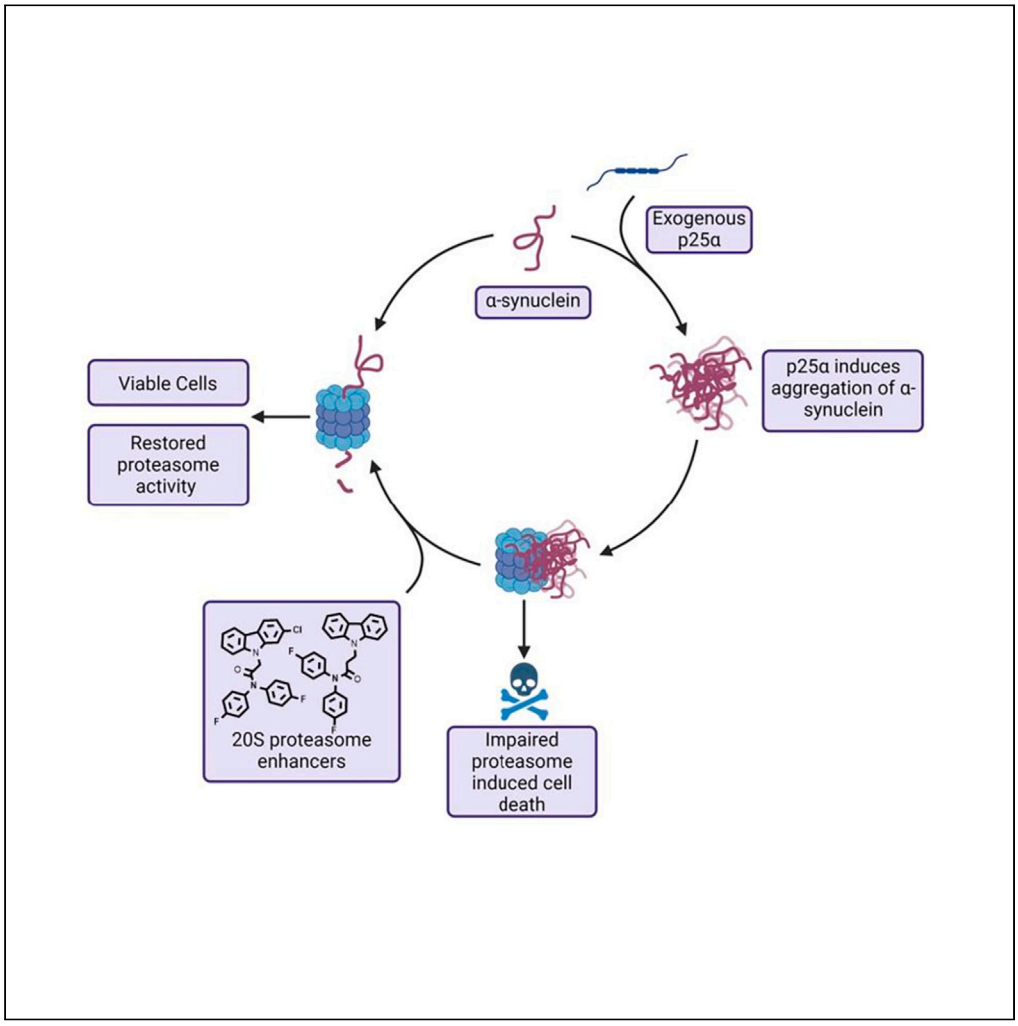

Sophia D. Staerz, Charles Anamoah, Jetze J. Tepe

tepe@virginia.edu

Highlights

p25α induced α-synuclein aggregation induces proteasome impairment

Identification of potent 20S proteasome enhancers

Proteasome enhancers reduce α-synuclein fibrillization

Proteasome enhancers prevent p25α/α-synuclein induced cytotoxicity

Staerz et al., iScience 27, 110166
July 19, 2024
https://doi.org/10.1016/j.isci.2024.110166

iScience

CellPress
OPEN ACCESS

Article

20S proteasome enhancers prevent cytotoxic tubulin polymerization-promoting protein induced α-synuclein aggregation

Sophia D. Staerz,[1,2] Charles Anamoah,[1] and Jetze J. Tepe[1,2,3,4,*]

SUMMARY

Synucleinopathies are a class of neurodegenerative diseases defined by the presence of α-synuclein inclusions. The location and composition of these α-synuclein inclusions directly correlate to the disease pattern. The inclusions in Multiple System Atrophy are located predominantly in oligodendrocytes and are rich in a second protein, p25α. P25α plays a key role in neuronal myelination by oligodendrocytes. In healthy oligodendrocytes, there is little to no α-synuclein present. If aberrant α-synuclein is present, p25α leaves the myelin sheaths and quickly co-aggregates with α-synuclein, resulting in the disruption of the cellular process and ultimately cell death. Herein, we report that p25α is susceptible for 20S proteasome-mediated degradation and that p25α induces α-synuclein aggregation, resulting in proteasome impairment and cell death. In addition, we identified small molecules 20S proteasome enhancers that prevent p25α induced α-synuclein fibrilization, restore proteasome impairment, and enhance cell viability.

INTRODUCTION

Multiple System Atrophy (MSA) and Parkinson's disease (PD) are members of a heterogeneous class of neurodegenerative disorders (NDDs), termed synucleinopathies, which share the characteristic presence of α-synuclein rich inclusions.[1,2] Primarily located in the presynaptic nerve terminals, the intrinsically disordered protein (IDP), α-synuclein, is proposed to regulate neurotransmitter release.[3,4] Under pathological conditions, α-synuclein accumulates throughout the cell and forms aggregates.[5,6] During this aggregation, α-synuclein forms toxic oligomeric species that disrupt several cellular pathways, including the ubiquitin-proteasome system (UPS).[7–9] The cell type bearing the α-synuclein deposits correspond to the differing disease patterns of PD and MSA.[10] Inclusions principally observed in neuronal cells are termed Lewy bodies and are associated with disorders such as PD.[11,12] α-synuclein inclusions localized in oligodendrocytes are termed glial cytoplasmic inclusions (GCIs) and are a hallmark of MSA.[13] Despite the prevalence of synucleinopathies, there are no approved disease-controlling therapeutics, and current treatments are limited to symptom management.[10,14] Targeting α-synuclein directly with small molecules has proven to be difficult, due to the flexible and dynamic nature of α-synuclein.[14,15]

The flexible nature of α-synuclein allows for the adoption of different conformations depending on the protein interacting with α-synuclein. The differing conformations then dictate the structure and the composition of the α-synuclein deposits, which play a significant role in the pathologies of the different synucleinopathies.[16,17] In addition, missense mutations of α-synuclein that increase the aggregation rate have been identified.[18] In particular, the A53T mutant α-synuclein has been linked to the aggressive familial form of PD and has been observed to be prion-like when introduced to MSA aggregates.[19,20]

Recently, α-synuclein aggregates derived from patients with PD and MSA were identified to structurally differ from one another.[16,17] MSA-derived α-synuclein strains present a higher degree of β-sheet structures,[16] and are significantly more toxic and resistant to protease degradation as compared to their PD-derived counterparts.[21] *In vivo* studies identified MSA-derived fibrils induce more severe neurodegeneration, neuroinflammation, and motor impairment.[22] The more aggressive seeding and spreading behavior of the MSA α-synuclein fibrils directly reflect the destructive nature of MSA.[22] The distinctive behavior and structure of the MSA-derived α-synuclein strains have been associated with the co-localization of an oligodendrocyte-specific IDP, tubulin polymerization promoting protein (TP/p25α), referred to as p25α hereafter.[23–26] Physiologically, p25α is solely expressed in oligodendrocytes and aids in neuronal myelination.[26,27] While the mechanism of α-synuclein entry into the oligodendrocytes is under debate, when present, p25α migrates from the myelin sheaths to the cell body,[22] causing loss of neuronal myelination and induces the rapid co-aggregation with α-synuclein.[23,28] The newly formed p25α/α-synuclein aggregates are then secreted out of the oligodendrocytes and enter surrounding neurons in a prion-like fashion, aiding in the spread of GCI-like inclusions.[29,30]

[1]Department of Chemistry, Michigan State University, East Lansing, MI 48824, USA
[2]Department of Pharmacology and Toxicology, Michigan State University, East Lansing, MI 48824, USA
[3]Department of Chemistry, University of Virginia, Charlottesville, VA 22904, USA
[4]Lead contact
*Correspondence: tepe@virginia.edu
https://doi.org/10.1016/j.isci.2024.110166

The UPS plays a vital role in cellular proteostasis and is responsible for the degradation of intracellular proteins, including IDPs and redundant or oxidatively damaged proteins.[31–34] The cell's main proteasome, the 26S proteasome, primarily degrades proteins in a ubiquitin-dependent manner. The 26S proteasome comprises a complex of one or two 19S regulatory particles (19S caps) and the 20S core particle, known as the 20S proteasome.[32]

The uncapped 20S proteasome is the default proteolytic enzyme responsible for the degradation of unfolded proteins without the need for ubiquitination.[35] When the basal activity of the proteasome isn't enough to combat the accumulation and aggregation of dysregulated IDPs, the pathogenesis of NDDs, such as PD and MSA, is triggered.

Recently, our group and others have identified small molecules[36–44] and peptides[45–47] capable of enhancing the proteolytic activity of the 20S proteasome, thereby reducing the cellular accumulation of IDPs.[36–41,48,49] We successfully designed a potent small molecule 20S proteasome enhancer based on the FDA-approved neuroleptic agent Chlorpromazine (CPZ),[39] where the dimethyl amine tail of CPZ was exchanged for *N,N*-bis(4-fluorophenyl)amide. However, the level of proteasome activation observed *in vitro* did not translate well in cellular studies. The core group of CPZ is a phenothiazine, which has been linked to both heavy metabolism and promiscuity.[50,51] We hypothesized that the lack of cellular efficiency may stem from the problematic nature of the phenothiazine motif. Therefore, we moved to synthesize novel small molecules with various heterocyclic cores containing the *N,N*-bis(4-fluorophenyl)amide tail.

The small molecules reported herein showed significantly improved cellular potency by preventing the accumulation of pathological A53T α-synuclein at < 1 μM concentrations. Furthermore, a simple proteasomal impairment model was developed to evaluate p25α induced aggregation of α-synuclein in cells. In these studies, we identified p25α as a substrate for 20S proteasome-mediated degradation and that p25α-induces α-synclein aggregation, resulting in proteasome impairment and cell death. In addition, we identified small molecule 20S proteasome enhancers that prevent p25α induced α-synuclein fibrilization, restore proteasome activity, and enhance cell viability. Whereas this model may not necessarily recapitulate disease pathogenesis seen in oligodendrocytes, it allows for the rapid screening and identification of small molecules capable of preventing p25α induced α-synuclein aggregation.

RESULTS

In vitro evaluation of 20S proteasome enhancers and molecular docking analysis

Compounds **1–20** were synthesized, as shown in Figure 1A and evaluated for 20S proteasome activity using a fluorogenic peptide assay. A fluorescent 7-amino-methyl coumarin (AMC) probe is conjugated to small peptides that mimic the preferred cleavage sites of each of the three catalytic sites of the 20S proteasome: Suc-LLVY-AMC (chymotrypsin-like site), Z-LLE-AMC (caspase-like site), and Boc-LRR-AMC (trypsin-like site).[42] When the peptides interact with the catalytic sites, the AMC probe is cleaved, releasing a fluorescent signal. This fluorescent signal is recorded every 5 min for an hour to determine the increase of the fluorescent signal over time, revealing the rate of peptide degradation by the 20S proteasome. We employed an equimolar mixture of the three fluorogenic peptide probes to evaluate the impact of the test compounds on overall 20S proteasome activity. The 20S proteasome was treated with various concentrations of the compounds and a vehicle control, and subsequently incubated at 37°C for 20 min. After incubation, a mixture of the three fluorogenic peptide probes (13.3 μM of each) was added, and the fluorescent output was recorded every 5 min for an hour. In a black 96-well plate, purified human 20S proteasome (0.5 nM)[39] was treated with 30 μM, 15 μM, 7.5 μM, and 3.75 μM of each test molecule in DMSO as vehicle or vehicle control only (final concentration 2%). The max-fold increase of the degradation rate was determined by calculating the treated proteasome degradation rate ratio over the untreated samples. The concentration where the degradation rate is enhanced 2-fold, or 200% (EC_{200}) was determined using a range of concentrations. Compounds observed to have an EC_{200} lower than 3.75 μM were tested in a 9-point concentration range (30 μM–0.16 μM).

The data collected from these studies are reported in Figure 1. Molecules containing a tricyclic heterocycle all displayed 20S proteasome activation, albeit in a range of max fold increases and EC_{200}. For this group of molecules, the impact of the methylene linker length was most evident when comparing the two carbazoles **1** and **2** (Figure 1B). The carbazole containing the two-methylene linker, compound **1**, was observed to be a potent and efficient 20S proteasome activator with a EC_{200} of 1.6 μM and a max fold increase of 5.8 at 30 μM. In contrast, compound **2**, the one-methylene-linked carbazole, displayed a weaker potency, with an EC_{200} of 3.8 μM. The change in the linker length was better tolerated when a 2-chlorocarbazole was used as the heterocyclic core and displayed an inverse trend compared to compounds **1** and **2**. The one-methylene-linked 2-chlorocarbazole (**4**) displayed a higher degree of 20S proteasome activation than its two-methylene counterpart (**3**) (Figure 1B). Compound **4** had an EC_{200} of 1.2 μM (max fold enhancement of 6.1), compared to compound **3**, which had an EC_{200} of 0.9 μM and a max enhancement of 20S proteasome activity of 4.5-fold. The carbolines **5** and **6** displayed similar potency, with an EC_{200} of 3.8 μM and 2.0 μM, respectively. However, the max fold of the two-methylene-linked carboline (**5**) (max-fold of 12) was twice that of the one-methylene counterpart (**6**) (max-fold of 5.5). Comparing the activities of these two sets of molecules suggests that the chlorine in the 2-position impacts how the molecules interact with the proteasome.

To understand how the chlorine impacts 20S proteasome activation, an unbiased molecular docking study was performed using Autodock Vina and Discovery Visualizer.[52,53] We have previously reported the use of molecular docking as a method to elucidate critical interactions between our small molecules and the pockets formed by the α-subunits.[37–39] We found that the 2-chlorophenothiazine linked to the bis(fluorophenyl) amide tail was predicted to favor the α 1/2 pocket of the α-ring of the 20S proteasome.[39] The preference for the α 1/2 pocket was observed for both the one-methylene linked carbazoles, compounds **2** and **4** (Figures 2A and 2B). This result was quite interesting due to their varying degrees of ability to activate the 20S proteasome. With the only difference between these two molecules being the chlorine in the 2-position, the preferred conformation and interaction points with the α 1/2 pocket and compounds **2** and **4** were further analyzed.

A

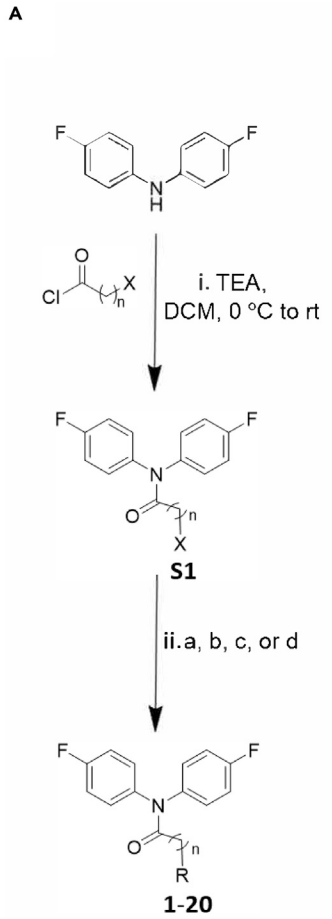

B

Comp. #	Heterocyclic core	n	Yield	Max Fold	EC_{200} (μM)
1	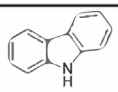	2	59%[a]	5.8 ± 1.4	1.6 ± 0.8
2		1	92%[a]	5.1± 1.1	3.8 ± 0.6
3	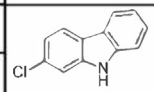	2	88%[a]	4.5 ± 1.2	0.9 ± 0.5
4		1	58%[a]	6.1 ± 2.7	1.2 ± 0.8
5	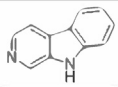	2	38%[a]	12.0 ± 2.6	3.8 ± 1.2
6		1	65%[a]	5.5 ± 2.2	2.0 ± 0.9
7		2	65%[a]	3.5 ± 0.9	7.5 ± 1.6
8		1	60%[a]	4.4 ± 1.2	7.5 ± 2.2
9	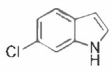	2	62%[a]	4.4 ± 2.7	0.9 ± 0.6
10		1	77%[a]	4.0 ± 1.4	1.6 ± 1.5
11		2	47%[b]	5.0 ± 0.4	9.0 ± 3.5
12		1	70%[b]	5.1 ± 0.9	8.0 ± 0.6
13	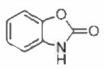	2	46%[c]	4.8 ± 1.1	1.3 ± 0.3
14		1	84%[c]	---	>30
15	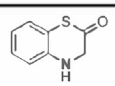	2	98%[a]	---	>30
16		1	80%[a]	4.3 ± 1.3	15 ± 3.3
17		2	36%[b]	---	>30
18		1	30%[b]	---	>30
19		2	64%[d]	---	>30
20		1	48%[d]	---	>30

Figure 1. Synthetic schemes and activity data of compounds 1–20

(A) Synthetic scheme for the synthesis of compounds 1–20. i. TEA, in DCM at 0°C and increased to room temperature, ii. (a) heterocyclic core, NaH, DMF at 0°C for 1 h and then room temperature for 24 h, (b) TEA in toluene, refluxed for 24 h, (c) K_2CO_3 in CH_3CN or DMF at 80°C for 24 h, (d) TEA in THF at room temperature for 24 h. (B) Table depicting the fold increase, denoted as max-fold, in 20S proteasome-mediated proteolysis induced by compounds 1–20 of an equimolar mixture of the Suc-LLVY-AMC, the chymotrypsin-like probe (CT-L), Z-LLE-AMC, the caspase-like probe (Casp-L), and Boc-LRR-AMC, the trypsin-like probe (T-L). The EC_{200} depicts the concentration at which the treated 20S proteasome exhibits a 200% enhancement of the rate of degradation of the small peptide substrate compared to the vehicle control. Values are mean ± standard deviation of $n = 3$ independent experiment.

The molecular docking results of compounds **2** and **4** were overlayed to compare their preferred binding conformation (Figure 2B). Compound **2** had the carbazole core pointed into the pocket with the bis(fluorophenyl) amide tail closest to CYS161, which was previously identified as a potential key interaction point for 20S proteasome activation, along with TYR159 (Figure 2C).[39] In comparison, compound **4** is predicted to have the 2-chlorocarbazole core directly parallel to TYR159 (Figure 2D). The *N,N*-bis(fluorophenyl) amide tail pointed into the pocket, with one fluorophenyl ring in proximity to CYS161. In contrast, the second fluorophenyl ring sits in the same orientation as the carbazole core of compound **2**. Consequently, the addition of chlorine flipped the predicted binding conformation, consistent with the changes observed in 20S proteasome activity.

Using BIOVIA Discovery Visualizer, the predicted interactions of compounds **2** and **4** and the α 1/2 pocket were compared (Figures 2C and 2D). Unsurprisingly, there were key differences in how compounds **2** and **4** interacted with the α 1/2 pocket. While both compounds interacted with CYS161 through a π-sulfur and π-alkyl interactions, compound **4** has an additional hydrogen bond between the -SH of CYS161 and the fluorine of the bis(fluorophenyl) amide tail. Although, this type of hydrogen bonding is considered a weak interaction, it has been observed to increase binding affinity.[54,55] In part, this may explain the difference in activity of compounds **2** and **4**.

In addition, compound **4** is predicted to interact differently with TYR159 and TYR75 than compound **2**. We had previously identified that molecules that interact with TYR159 through one mode of π – π stacking displayed little to no 20S proteasome activation.[39] Compound **2**

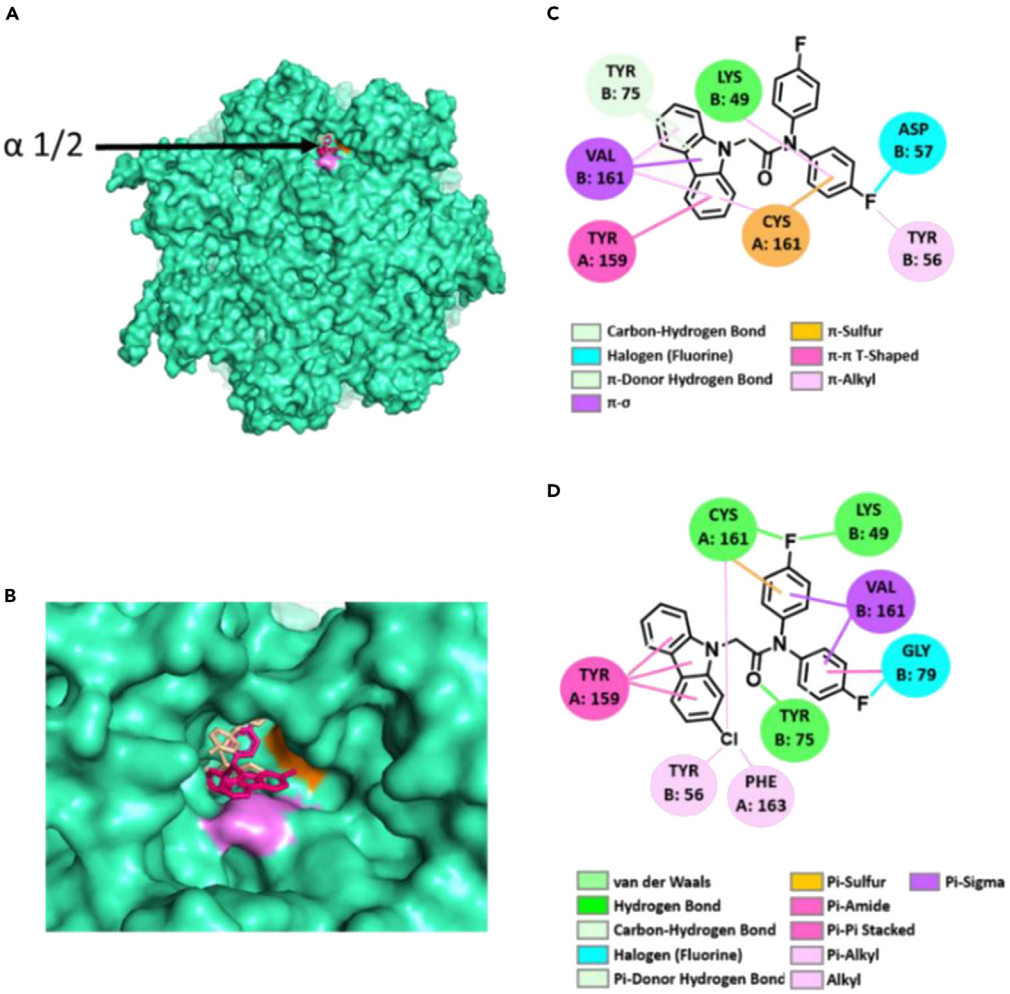

Figure 2. Preferred predicted docking modes of the compounds with the 20S proteasome

Preferred binding pocket of compounds (A) 2 (wheat) and 4 (pink). (B) Overlay of predicted confromation of compounds **2** (wheat) and **4** (pink) in the α 1/2 pocket with the location of TYR159 highlighted in light-pink and CYS161 highlighted in orange. The predicted binding interactions of compounds (C) **2** and (D) **4**.

interacts with TYR159 through only a π - π T-shaped interaction. In contrast, compound **4** is predicted to have three π – π interactions with TYR159. Lastly, the interactions with TYR75 are of note. Compound **2** interacts with TYR75 through a weak π-donor hydrogen bond as compared to the stronger C=O···H-O for compound **4**.[56] Compound **4** interacts with CYS161 and TYR159 in a manner that is in agreement with our previous studies.[39]

In addition, the strong hydrogen bonding with TYR75 may explain the potent nature of compound **4**. In contrast to the tricyclic-containing molecules, the bicyclic molecules were generally less efficient and less potent. Only one bicyclic compound, **9**, had an EC_{200} below 1 μM. Compound **9**, a two-methylene-linked 2-chloroindole, was observed to be a potent 20S proteasome activator with an EC_{200} of 0.9 μM and a max fold increase of 4.4. The one-methylene-linked 2-chloroindole (**10**) was as efficient as compound **9** (EC_{200} of 1.6 μM versus 0.9 μM, respectively). Compounds **7** and **8** displayed an identical EC_{200} of 7.5 μM and similar 20S proteasome activation efficiencies with max folds of 3.5 and 4.4, respectively. These indoles were also predicted to bind to the α 1/2 pocket and interacted with CYS161 through a π-alkyl interaction. It was previously observed that molecules interacting in this manner displayed weaker EC_{200} and max folds.[39]

The incorporation of hydrogen bond acceptors was beneficial when connected to the two-methylene linker (**13**, EC_{200} of 1.3 μM) but abrogated all 20S proteasome activity when coupled with the one-methylene linker (**14**). Compound **14** completely lacked any interaction with TYR159. This finding agrees with our previous assessment that an interaction with TYR159 is important for 20S proteasome activation.[39] The additional flexibility in some bicyclic ring analogs (**11** and **12**) reduced potency, displaying EC_{200} of 9.0 μM (**11**) and 8.0 μM (**12**). However, the complete elimination of the aromatic group in the heterocyclic core abolished all 20S proteasome activity, as seen with compounds **17**–**20**. Next, molecules that had an EC_{200} of below 1 μM were carried forward. The corresponding methylene linker pairs were also included as a negative control or to further evaluate the linker length's impact on 20S proteasome activation with physiologically relevant proteins.

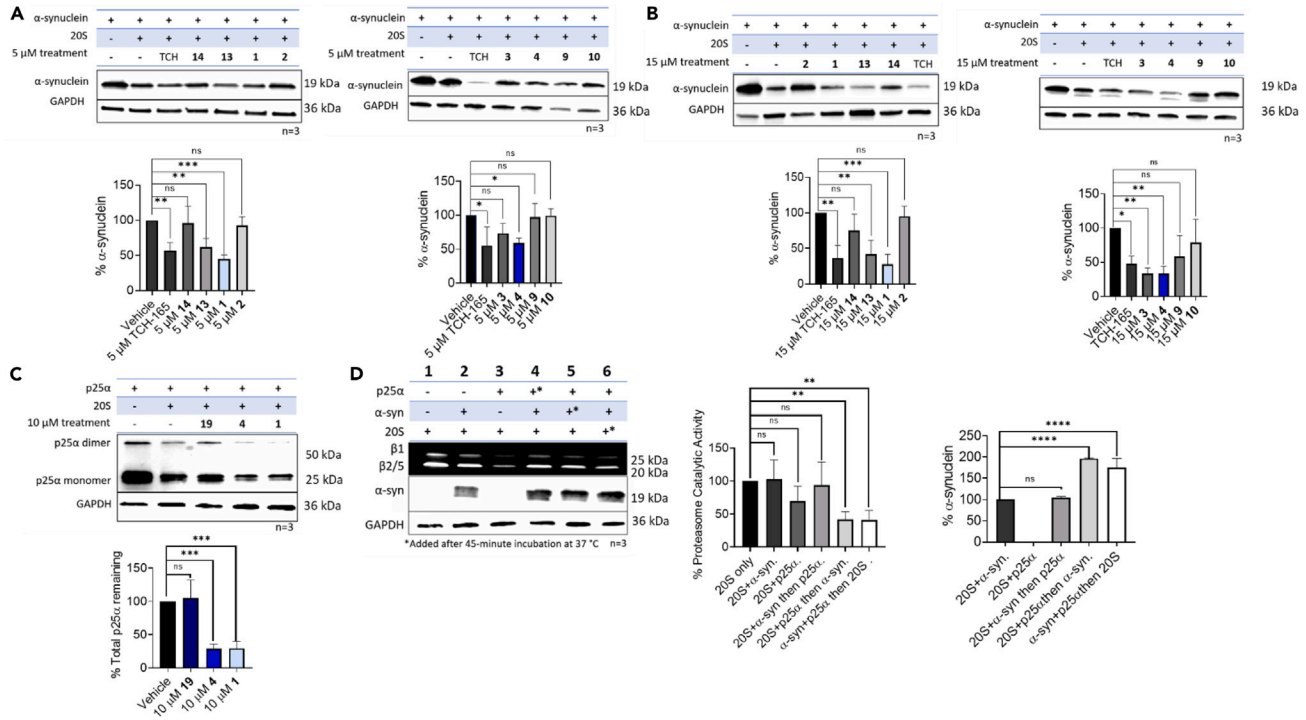

Figure 3. *In vitro* evaluation of p25α and α-synuclein degradation and impact of p25α/α-synuclein co-incubation on 20S proteasome activity

(A and B) The degradation of purified α-synuclein by the 20S proteasome treated with (A) 5 μM and (B) 15 μM of compounds **1**–**4**, **9**, **10**, **13**, **14**, or the postive control, TCH-165. GAPDH was added as a loading control.

(C) The degradation of purified p25α by the 20S proteasome treated with 15 μM of compounds **1** and **4**.

(D) Proteasomal impairment by p25α/α-synuclein aggregates, visualized using Me4BodipyFL-Ahx3Leu3VS probe in an SDS-PAGE gel and levels of α-synuclein using immunoblotting. Each set of assays were done in triplicate. Error bars denote standard deviation. One-way ANOVA statistical analysis was used to determine statistical significance (ns = not significant, *$p < 0.05$, **$p < 0.01$, ***$p < 0.001$, ****$p < 0.0001$). Error bars based on standard deviation. n denotes number of replicates.

N,N-bis(4-fluorophenyl)amide analogs enhance the degradation of purified α-synuclein

Given the number of molecules exhibiting a low EC_{200}, two concentrations of each compound were evaluated (5 μM and 15 μM). The 20S proteasome activator, TCH-165,[41] was used as a positive control, and DMSO-treated 20S proteasome functioned as the vehicle control. Purified 20S proteasome was diluted in a 50 mM HEPES and 5 mM DTT buffer (pH 7.2, 10 nM final concentration).[39,40,57] The desired concentration of **1**-**4**, **9**, **10**, **13**, and **14** or the control compound, TCH-165, was added to the proteasome solution and incubated for 45 min at 37°C. Then, purified α-synuclein was added (300 nM final concentration). The protein digestion was incubated at 37°C for 3.5 h. The remaining full-length α-synuclein was visualized and quantified using immunoblotting (Figures 3A, 3B, S2A, S2B, S3A, and S3B). TCH-165 enhanced the 20S proteasome-mediated degradation of α-synuclein at both concentrations with an average of 60% and 40% α-synuclein remaining at 5 μM and 15 μM, respectively. At 15 μM, several compounds outperformed TCH-165, but two compounds, **1** and **4**, outperformed TCH-165 at the lower concentration of 5 μM. Proteasome treated with 5 μM and 15 μM of **1** displayed an enhanced degradation of α-synuclein with 45% and 28% α-synuclein remaining, respectively (Figures 3A, 3B, S2A, S2B, S3A, and S3B). Furthermore, the two potent 2-chlorocarbazole molecules (**3** and **4**), performed very similarly to **1** at 15 μM with only 33% α-synuclein remaining. Compound **4** performed worse than compound **1** at 5 μM (58% remaining, Figures 3B, S2A, S2B, S3A, and S3B). Due to their ability to enhance the degradation of α-synuclein at both concentrations, **1** and **4** were carried forward for further evaluation.

p25α identified as a direct 20S proteasome substrate and compounds 1 and 4 enhance this degradation

It has been previously identified that p25α can be degraded through both autophagy and the UPS.[23,58–60] The ability of the 20S proteasome to degrade p25α has yet to be determined. To help elucidate the potential mechanism of proteasome enhancement in the intervention of synucleinopathies, the ability of purified 20S proteasome to degrade p25α was investigated. The 20S proteasome (final concentration of 7.5 nM) was added to a 120 mM NaCl, 50 mM Tris, and 0.1% β-mercaptoethanol buffer (pH 7.4).[61] The proteasome was treated with either DMSO or 10 μM of **1**, **4**, or an inactive analog, **19,** at 37°C while purified p25α was separately incubated with 100 μM of DTE at room temperature, for 30 min. The purified p25α (final concentration of 500 nM) was added to the proteasome:drug solution for 3 h. The DMSO-treated 20S

proteasome decreased the amount of p25α drastically (Figures 3C and S4), suggesting p25α is a 20S proteasome substrate. In addition, **1** and **4** were both able to increase the rate of degradation of purified p25α with 29% and 28% p25α remaining, respectively, as compared to the DMSO treated samples (Figures 3C and S4). Inactive control, **19**, didn't show significant impact on the rate of p25α degradation.

Interaction between p25α/α-synuclein impairs 20S proteasome activity *in vitro*

IDP aggregates have been identified to impair the activity of the proteasome *in vitro*[8] and in cells.[48] After we identified p25α as a 20S proteasome substrate, we moved to evaluate if p25α/α-synuclein interaction can cause proteasomal impairment. All samples were prepared in the same manner, with two incubation points (45 min followed by 3 h, both at 37°C). After these incubation times, a covalent Me4BodipyFL-Ahx3Leu3VS fluorescent probe was added, and the samples were further incubated at 37°C for 15 min.[62] The probe was selected to visualize the activity of the 20S proteasome using a denaturing gel (Figures 3D and S5). The remaining levels of α-synuclein were then visualized through an immunoblot, and GAPDH was used as a loading control. Due to the low concentration of p25α used, the remaining levels could not be visualized. The activity of the 20S proteasome in each sample is depicted in Figures 3D and S5, with each lane representing a different combination and order of addition of 20S, PBS, p25α, and α-synuclein. Lane 1 depicts the activity of the 20S proteasome first treated with PBS for 45-min, then treated with PBS for the 3-h incubation. Samples in lane 1 were used as the vehicle control. Samples in lane 2, were first treated with 700 nM of α-synuclein, followed by the addition of PBS. The activity displayed by the samples in lane 2 had no significant difference as compared to the vehicle control. The activity of the 20S proteasome in samples that were first treated with 150 nM of p25α, followed by the addition of PBS, are shown in lane 3. While there was a noticeable trend of reduced proteasome activity in these samples, after the experiment was triplicated, this trend was identified to be non-significant. In lane 4, the 20S proteasome was treated first with 700 nM of α-synuclein, followed by the addition of 150 nM of p25α after the first incubation. After the 3-h incubation, the activity of the 20S proteasome had no significant change as compared to the vehicle in lane 1. Inversely, lane 5 represents the activity of the 20S proteasome when treated first with 150 nM of p25α, followed by the addition of 700 nM of α-synuclein. These samples showed a significant decrease in proteasome activity, with 36% activity remaining. This decline in activity was corroborated by the decline in α-synuclein degradation (197%) as compared to lane 2 (Figures 3D and S5). The final lane, 6, 700 nM of α-synuclein and 150 nM of p25α were added together for the first 45-min incubation. The 20S proteasome was then added for the 3-h incubation. Similar to lane 5, samples in lane 6 displayed impaired proteasome activity, with 41% activity remaining. The degradation of α-synuclein was also prevented, with 175% α-synuclein compared to lane 2 samples (Figures 3D and S5).

Compounds 1 and 4 enhance the cellular degradation of A53T α-synuclein

We evaluated if the enhanced 20S proteasome activity by compounds **1** and **4** translated in cellular conditions. HEK-293T cells were transiently transfected with an A53T α-synuclein plasmid. The A53T α-synuclein plasmid was used due to its increased aggregative properties.[5,62,63] After 48 h of protein expression, the HEK-293T cells were treated with four concentrations of **1** and **4** (1, 5, 10, and 15 μM) for 16 h and then lysed. The levels of A53T α-synuclein were visualized and quantified using immunoblotting (Figures 4A, 4B, S6, and S7). Samples were treated with 10 μM of TCH-165 as a positive control, 15 μM of the structurally related inactive analog **14**, 30 nM of a proteasome inhibitor Bortezomib (BTZ) as a negative control, and DMSO as a vehicle control (Figures 4A, 4B, S6, and S7).

Samples treated with compound **1** showed a significant reduction in A53T α-synuclein as compared to the vehicle, at all concentrations tested. The degree to which **1** was able to prevent A53T α-synuclein accumulation was clearly dose-dependent. At the lowest concentration, 1 μM, there was 64% of A53T α-synuclein remaining, while at the highest concentration of 15 μM, there was 21% A53T α-synuclein remaining (Figures 4A and S6). TCH-165 (10 μM) had 52% A53T α-synuclein remaining. While the inactive control (**14**) had no significant effect on degradation, and BTZ did increase the levels of A53T α-synuclein by 148% via proteasome inhibition (Figures 4A and S6). In a similar trend, **4** performed as well as, if not better than, **1**. Cells treated with 1 μM of **1** had a 67% decrease of A53T α-synuclein. Compound **4** outperformed **1** at 5 μM, preventing the accumulation of A53T α-synuclein (30% remaining) (Figures 4B and S7). The reduction of A53T α-synuclein at 10 μM and 15 μM were extremely close with only 14% and 11% A53T α-synuclein remaining, respectively. The TCH-165 positive control prevented accumulation with an average of 40% A53T α-synuclein remaining. The inactive control, **14**, continued to have no impact on the levels of A53T α-synuclein, and the negative control BTZ increased A53T α-synuclein levels by 135% (Figures 4B and S7).

The potency displayed by **1** and **4** in the fluorogenic peptide assay readily translated to cellular conditions. Due to the levels of activity shown by **1** and **4** at 1 μM we explored the cellular activity at lower concentration (Figure S8). Samples treated with compounds **1** and **4** displayed enhanced degradation of A53T α-synuclein at sub-micromolar concentrations. When treated with 0.75 μM of compounds **1** and **4** displayed 55% and 72% of α-synuclein remaining, Figure 4D, respectively.

Compound 1 enhances the degradation of p25α in HEK-293T cells

The impact of 20S proteasome enhancement on p25α levels was investigated next. HEK-293T cells were transiently transfected with a p25α plasmid for 48 h before treatment with 10 μM of **1**, **4**, and **19** for an additional 16 h. Compound **19** was substituted for compound **14** as the inactive control, due to the accessibility of compound **19**. Previous studies have found proteasome inhibitors increase the levels of p25α in cells.[23] As a control, samples were treated with 30 nM of BTZ (Figures 4C and S9). While there was a slight decrease in p25α levels in the HEK-293T cells treated with **4**, this decrease was identified as non-significant when triplicated. Samples treated with 10 μM of compound **1** had a 45% reduction of p25α. This activity contrasts the much more efficient 20S-mediated degradation of A53T α-synuclein induced by compound **1** (<1 μM). The inactive control compound, **19**, didn't impact the levels of p25α. The samples treated with proteasome inhibitor, BTZ,

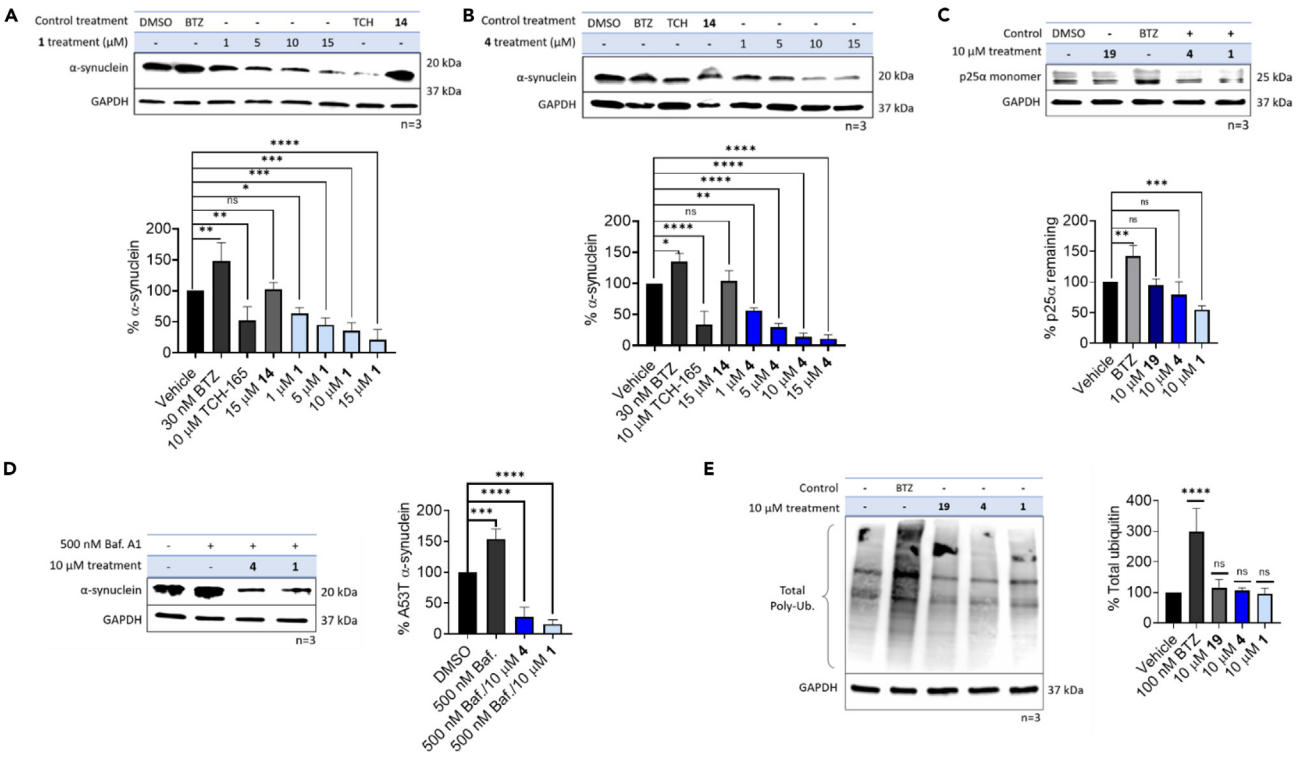

Figure 4. Compounds 1 and 2 enhance the degradation rate of cellular p25α and α-synuclein through a ubiquitin-dependent manner

(A and B) The evaluation of A53T a-synuclein levels in HEK-293T cells once they have been treated with 1, 5, 10, or 15 μM of compounds (A) **1** and (B) **4**, and with 15 μM of an inactive control, **14**, 10 μM of a positive control, TCH-165, and 30 nM of a proteasome inhibitor, BTZ.

(C) Quantification of levels of p25α in HEK-293T cells treated with 10 μM of compounds **1** and **4**.

(D) Levels of A53T α-synuclein in HEK-293T cells were pre-treated with 500 nM of Bafilomycin A1 and 10 μM of either compound 1 or 4.

(E) Ubiquitin levels in HEK-293T cells treated with 10 μM of compounds **1**, **4**, and **19**. The quantification of the target protein remaining was normalized using the GAPDH levels and compared to a DMSO-treated control. Each set of assays was done in triplicate. Error bars denote standard deviation. One-way ANOVA statistical analysis was used to determine statistical significance (ns = not significant, *$p < 0.05$, **$p < 0.01$, ***$p < 0.001$, ****$p < 0.0001$). Error bars based on standard deviation. n denotes the number of replicates.

displayed a modest 142% increase of p25α compared to the DMSO-treated samples (Figures 4C and S9). When the degradation of p25α was evaluated in PC12 cells, both compounds **1** and **4** could also enhance the 20S proteasome-mediated degradation of p25α at relatively high (10 μM) concentrations (Figure S10). Compound **1** outperformed compound **4**, with 40% and 67% p25α remaining. These data indicate that significantly higher concentrations of the compounds are needed to enhance p25α degradation compared to α-synuclein degradation.

Compounds 1 and 4 enhance the degradation of p25α and A53T α-synuclein through the ubiquitin-independent pathway

It has been reported that p25α/α-synuclein aggregates can be degraded through the autophagy pathway.[23] To validate that compounds **1** and **4** prevent the accumulation of α-synuclein through the UPS, the HEK-293T cells were transfected with the A53T α-synuclein plasmid. Following the 48-h protein expression period, the cells were treated with 500 nM of an autophagic flux inhibitor, Bafilomycin A1,[64] for 1 h before treatment with 10 μM of **1** and **4** (Figures 4D and S11). Both compounds enhanced the degradation of A53T α-synuclein (16% and 28% remaining, respectively) despite the pretreatment with Bafilomycin A1, suggesting the UPS is the main target of modulation for this class of small molecules. We, next, sought to identify if the compound modulation of the UPS was specific to the 20S proteasome or if the molecules impacted the ubiquitin-dependent pathways. Unmodified HEK-293T cells were treated with 10 μM of **1**, **4**, and **19** as well as 100 nM of BTZ, and the levels of ubiquitin were visualized and quantified using immunoblotting (Figures 4E and S12). Unsurprisingly, BTZ treated samples had 298% ubiquitin as compared to the vehicle. While **1**, **4**, and **19** didn't impact the levels of ubiquitin significantly. Further supporting **1** and **4** modulating the activity of the ubiquitin-independent pathway.

Compounds 1 and 4 avert α-synuclein aggregation induced by extracellular p25α

It's been demonstrated that purified p25α and α-synuclein can be taken up by cells through media.[23,65,66] The co-enrichment of the two IDPs then led to aggregation, mimicking the pathological state. The pheochromocytoma of the rat adrenal medulla cells, PC12, has been previously used to evaluate the impact of α-synuclein aggregates in cellular systems.[67,68] Furthermore, PC12 cells have been identified to take up

IDPs from the media,[69] making them an ideal cell line to observe the impact of extracellular p25α on cellular α-synuclein. Using PC12 cells transfected with the A53T α-synuclein plasmid, we investigated the impact of 20S proteasome enhancement on p25α-induced α-synuclein aggregation. PC12 cells were transfected with the A53T mutant plasmid, and the protein was expressed for 48 h. To investigate whether our small molecules assist in the prevention of this aggregation, cells were treated with 10 μM of **1**, **4**, and **19** for 2 h and then treated with purified p25α (final concentration of 160 nM) for an additional 24 h. PC12 cells that were either not transfected, only expressed A53T α-synuclein, or just treated with purified p25α were included as controls. The PC12 cells were plated in a black opaque-bottom 96-well plate (10,000 cells/well).

To each well in the 96-well plate, 800 nM of the RB1 probe[70] was added to evaluate the degree of α-synuclein fibrillization. The change in fluorescence observed is attributed to the degree of aggregation and fibrillization of α-synuclein. PC12 cells that only expressed A53T α-synuclein showed no significant increase in RB1 fluorescence compared to the unmodified vehicle. In contrast, cells treated with p25α had a 234% increase in the observed fluorescence (Figures 5A and S14). The fluorescence observed in the non-transfected cells was attributed to the basal levels of α-synuclein expressed in PC12 cells. However, this increase in α-synuclein fibrillization associated fluorescence was relatively mild compared to the samples expressing A53T α-synuclein with p25α treatment, which showed an increase of 512%. When these cells were treated with **1** and **4**, there was a significant reduction in α-synuclein fibrillization, with 157% and 173% fluorescent signal remaining. The inactive analog **19** showed no impact on fibrillization levels.

Compounds 1 and 4 prevent p25α/α-synuclein-induced proteasomal impairment

The degree of fibrillization was then related to proteasome function by utilizing a luciferase-based assay, Proteasome Glo, to quantify the overall cellular proteasome activity. In contrast to the fibrillization studies, cells treated with p25α didn't display a significant alteration of proteasome activity (Figure 5B with raw data shown in Figure S15). A 42% reduction in proteasome activity was observed in PC12 cells expressing A53T α-synuclein and were exposed to purified p25α. Both compounds **1** and **4** restored proteasomal activity to 86% and 70%, respectively. These results were further supported by the levels of A53T α-synuclein and ubiquitin present in each sample (Figures 5C and S13). The remaining cells were lysed, and A53T α-synuclein and ubiquitin levels were visualized and quantified via immunoblotting (Figures 5C and S13). Samples, where both α-synuclein and p25α were present, displayed 155% of α-synuclein and 148% of ubiquitin as compared to the vehicle sample. **1** and **4** were again able to reduce the levels of both. Cells treated with **1** and **4**, reduced the levels of α-synuclein (39% and 48% remaining, respectively) and both restored ubiquitin levels (Figures 5C and S13).

Compounds 1 and 4 prevent cell death of A53T α-synuclein expressing PC12 cells that are exposed to p25α

Next, we evaluated the ability of compounds **1** and **4** to prevent p25α-induced cell death in A53T α-synuclein expressing PC12 cells. PC12 cells were plated in a white 384 well-plate (2,500 cells/well) and then immediately transfected with the A53T α-synuclein plasmid for 24 h. The PC12 cells were then treated with 3 μM of **1**, **4**, and **19.** The cells were also treated once every 24 h with purified p25α (160 nM daily concentration) for 72 h. Cell Titer Glo was used to assess the cell viability. Cells solely expressing A53T α-synuclein had a cell viability of 61%, while cells repeatedly treated with p25α showed significant cell death (28% cell viability) (Figure 6A with raw data shown in Figure S16). Only **1** prevented the cell death in the PC12 cells, with 72% cell viability, while **4** and **19** could not rescue the cells systematically treated with p25α (Figure 6A with raw data shown in Figure S16). The inability of **4** to prevent cell death in this system can be related to compound **4**'s moderately enhanced 20S proteasome-mediated degradation of p25α displayed both in HEK-293T and PC12 cells.

Compounds 1 and 4 protect cells from proteasomal impairment caused by cytotoxic p25α induced A53T α-synuclein aggregates, preventing cell death

With the observed impairment of the proteasome, the cytotoxicity of the p25α – induced A53T α-synuclein aggregates was evaluated. Furthermore, we wanted to evaluate if proteasome enhancers could prevent the observed cytotoxicity. Previous studies have suggested MSA-like aggregates are cytotoxic through the co-transfection of α-synuclein and p25α plasmids.[71] Using a similar co-transfection protocol, PC12 and HEK-293T cells were plated in a white 384-well plate (2,500 cells/well), co-transfected with the two plasmids for 24 h and then treated with 3 μM of **1**, **4**, and **19** for 72 h. The cell viability was then quantified using Cell Titer Glo (Figure 5B with raw data shown in Figure S17). In a second 384-well plate, the overall proteasome activity was again measured using Proteasome Glo (Figure 6C with raw data shown in Figure S18). The co-transfected PC12 cells displayed a 25% cell viability and 8% proteasome activity remaining, which was lower than the vehicle and cells transfected with either one of the plasmids. The co-transfected cells treated with **1** and **4** increased the cell viability to 76% and 75%, respectively (Figures 6B and S17). The proteasome activity in these samples increased, with **1** displaying 29% activity and **4** showing 34% remaining activity (Figures 6C and S18). The cytotoxicity was observed in HEK-293T cells as well; however, it became apparent that HEK-293T cells were much more sensitive to the co-expression of the two proteins, with a 17% cell viability remaining, with a significantly reduced plasmid load and treatment time. (Figures S19 and S20).

DISCUSSION

The diverse class of synucleinopathies share the presence of α-synuclein rich inclusions,[1,2] which toxic oligomeric species are formed capable of disrupting vital cellular pathways, such as the UPS.[8,37] MSA derived α-synuclein strains have been identified to be the most toxic and aggressive form of α-synuclein aggregates.[16,21,22] The α-synuclein inclusions identified in MSA often co-localize with a second IDP,

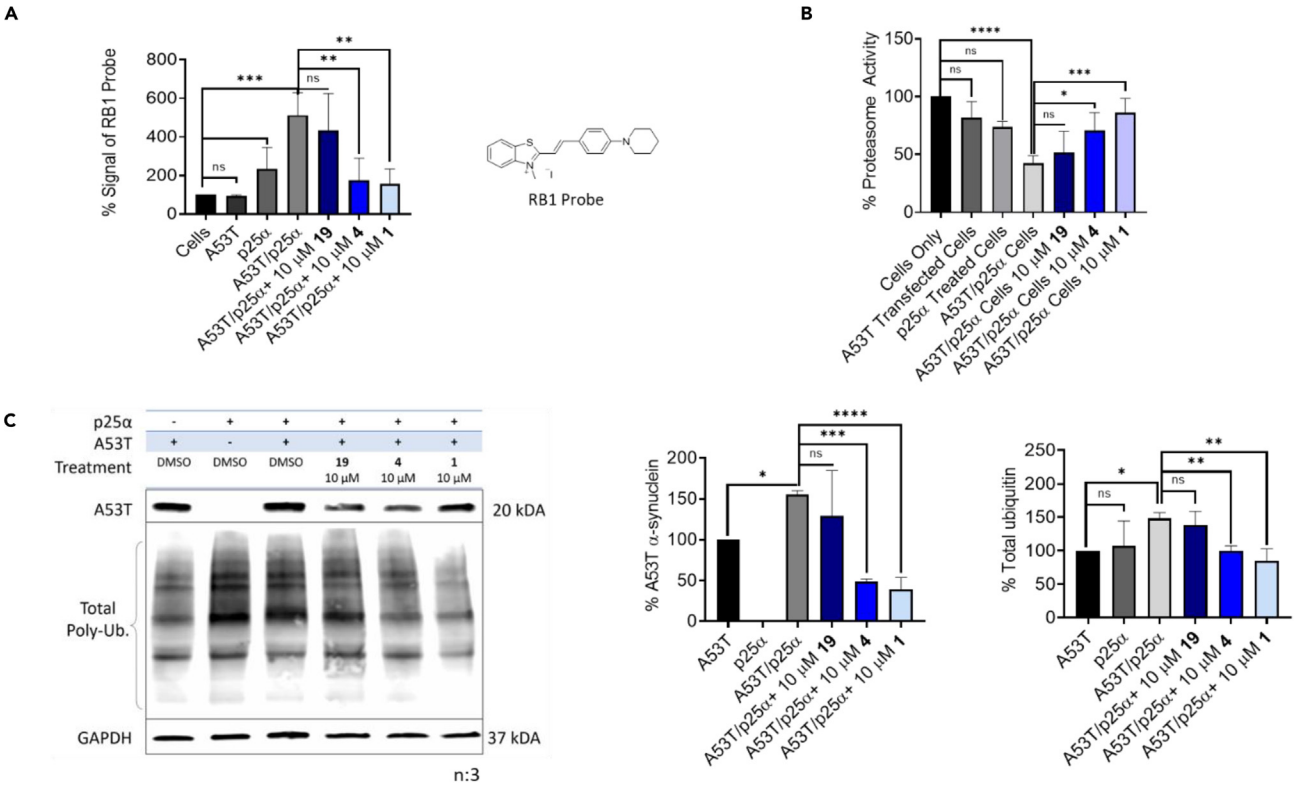

Figure 5. Compounds 1 and 4 lower the formation of p25α induced A53T α-synuclein aggregates and restored impair the activity of the cellular proteasomal activity

(A) The impact of 160 nM of purified p25α addition on A53T α-synuclein fibrillization in PC12 after a 2-h incubation with 10 μM of compounds **1**, **4**, and **19** quantified using the fluorescence of the RB1 probe.

(B) The proteasome activity in PC12 cells that express A53T α-synuclein when cells are first treated with 10 μM of compounds **1**, **4**, and **19** for 2 h and then 160 nM of purified p25α, as presented by a luminescent signal using the luciferase-based assay, Proteasome Glo.

(C) Immunoblots of A53T α-synuclein and ubiquitin in PC12 cells were treated with 10 μM of compounds **1**, **4**, or **19** for 2 h before adding 160 nM of purified p25α. The quantification of the target protein remaining was normalized using the GAPDH levels and compared to a DMSO-treated control in triplicate. Each set of assays was done in triplicate. Error bars denote standard deviation. One-way ANOVA statistical analysis was used to determine statistical significance (ns = not significant, *$p < 0.05$, **$p < 0.01$, ***$p < 0.001$, ****$p < 0.0001$). Error bars based on standard deviation. n denotes the number of replicates.

p25α.[24–26,72,73] Reports indicate that both p25α and α-synuclein can be degraded through either autophagy or the UPS.[23,58–60] Herein we have demonstrated that the 20S proteasome also contributes to α-synuclein and p25α degradation. Furthermore, we have synthesized a class of potent 20S proteasome enhancers (compounds **1** and **4**) capable of enhancing the degradation of both IDPs *in vitro* and in cells. The effect of small molecule 20S proteasome enhancement on p25α-induced α-synuclein aggregation, proteasome impairment, and cell viability were investigated. PC12 cells expressing A53T α-synuclein treated with purified p25α displayed a significant increase in α-synuclein fibrillization; however, the addition of the 20S proteasome enhancers, compounds **1** and **4**, significantly reduced this fibrillization (Figure 5A). Concurrent with the increase of p25α induced α-synuclein fibrillization, there was a significant proteasomal impairment (58% reduction in proteasome activity). Our data showed that 20S proteasome enhancement by compounds **1** and **4** prevented and rescued cells from proteasomal impairment (Figure 4B). Furthermore, PC12 cells co-expressing both p25α and A53T α-synuclein for 96 h showed 24% cell viability, and only 8% total proteasome activity remaining. Both 20S proteasome enhancers, **1** and **4**, were able to significantly restore cell viability (Figure 5B) and proteasome activity (Figure 5C).

Treatment of A53T α-synuclein expressing PC12 cells with purified p25α for 72 h, displayed 28% cell viability, which was restored to 75% viability, upon treatment with compound **1** (Figure 5A). While both compounds **1** and **4** displayed 20S proteasome-mediated degradation of α-synuclein (<1 μM) at low concentrations and p25α at higher concentrations (~10 μM), compound **4** was significantly less effective in inducing purified p25α degradation than compound **1**. This selectivity could explain the differing degrees of cytoprotection seen for compounds **1** and **4** when purified p25α (Figure 5A) versus cellular p25α in the co-transfection (Figure 5B).

We have discovered p25α as a new 20S proteasome substrate through these studies. In addition, p25α-induced aggregation of α-synuclein impairs the proteasome both *in vitro* and in cells and induces significant cell cytotoxicity. Treatment of the cells with 20S proteasome enhancers **1** and **4** prevents p25α-induced α-synuclein fibrillization, proteasome impairment, and cell cytotoxicity, indicating a potential new therapeutic strategy to treat p25α induced α-synuclein associated pathologies.

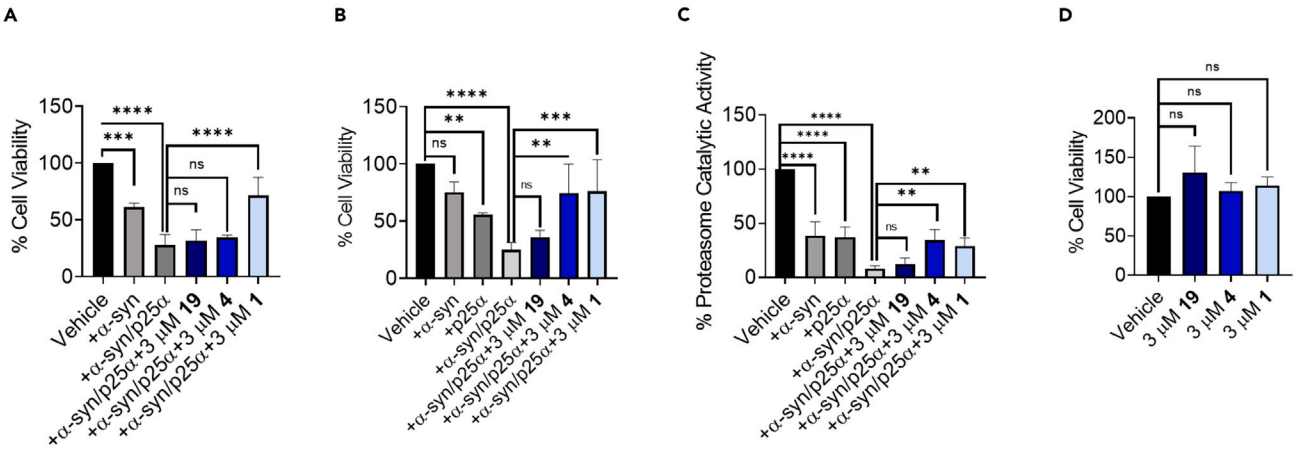

Figure 6. Compounds 1 and 4 restore proteasome activity and associated cytotoxicity in cells expressing p25α and α-synuclein

(A) The cell viability of PC12 cells that were transfected with an A53T α-synuclein plasmid for 24 h before the one-time treatment of 3 μM of compounds **1**, **4**, and **19** and a daily treatment of 160 nM of purified p25α for three days.

(B) The cell viability and (C) proteasome activity of PC12 cells that were co-transfected with a p25α and an A53T α-synuclein plasmid for 24 h before treatment with 3 μM of compounds **1**, **4**, and **19**.

(D) The toxicity of the compounds in unmodified PC12 cells. Each set of assays was done in triplicate. Error bars denote standard deviation. One-way ANOVA statistical analysis was used to determine statistical significance (ns = not significant, *$p < 0.05$, **$p < 0.01$, ***$p < 0.001$, ****$p < 0.0001$). Error bars based on standard deviation.

Limitations of the study

We validated 20S proteasome enhancers as a potential new therapeutic approach to neurodegenerative diseases (NDDs) using a cellular model that recapitulates the aggregation seen in synucleinopathies. However, there are a few limitations to our study. NDDs have extremely complex pathologies, and several impaired cellular pathways have been linked to NDD progression. This study focuses on the relationship between the proteasome and p25α/α-synuclein aggregates and does not evaluate the impact of these aggregates on other cellular pathways. Furthermore, immortalized cell lines were used to evaluate the impact of p25α/α-synuclein aggregates on cellular proteasome activity. Further evaluation of this model in primary oligodendroglial cells would be a valuable follow-up study. *In vivo* translational studies would further expand upon our findings and their impact on p25α induced α-synuclein aggregates, UPS, and other cellular pathways.

STAR★METHODS

Detailed methods are provided in the online version of this paper and include the following:

- KEY RESOURCES TABLE
- RESOURCE AVAILABILITY
  - Lead contact
  - Materials availability
  - Data and code availability
- EXPERIMENTAL MODEL AND STUDY PARTICIPANT DETAILS
  - Mammalian cell line
  - Bacteria cell culture
- METHOD DETAILS
  - Cell culture
  - Antibodies
  - Protein purification
  - Transfection and immunoblotting
  - Fluorogenic small peptide assay with purified 20S proteasome
  - Purified α-synuclein digestion with 20S proteasome
  - Purified p25α digestion with 20S proteasome
  - Purified 20S proteasome impairment by p25α/α-synuclein aggregates
  - P25α induced α-synuclein fibrillization and proteasome impairment in PC12 cells
  - Proteasome Glo
  - Cytotoxicity

- Systematic treatment with purified p25α
- Chemistry

- QUANTIFICATION AND STATISTICAL ANALYSIS

SUPPLEMENTAL INFORMATION

Supplemental information can be found online at https://doi.org/10.1016/j.isci.2024.110166.

ACKNOWLEDGMENTS

The authors gratefully acknowledge financial support from the National Institutes of Health, National Institute on Aging and National Institute of Neurological Disorders and Stroke. The authors would also like to extend gratitude toward Sydney Cobb for her helpful discussions during the writing process. National Institutes of Aging, R21 AG061306 (JJT), R21 AG076994 (JJT), and National Institute of General Medical Sciences, T32GM092715 (SDS) of the National Institutes of Health.

AUTHOR CONTRIBUTIONS

S.D.S synthesized compounds **1**, **3**, **4**, **5–9**, **11**, **12**, and **17–20**, performed molecular docking studies, performed purified enzymatic assays, performed two replicates of each of the *in vitro* α-synuclein assays, and two replicates of each of the cellular assays. S.D.S conducted all studies which p25α was included. C.A. synthesized compounds **2**, **6**, **10**, and **13–16**, performed molecular docking studies and performed the remaining replicates of the α-synuclein *in vitro* and cellular assays. C.A. purified p25α. The article was written through contributions of all authors. All authors have given approval to the final version of the article.

DECLARATION OF INTERESTS

JT declares a competing interest due to his involvement with Portera Therapeutics INC.

Received: October 10, 2023
Revised: February 5, 2024
Accepted: May 30, 2024
Published: June 4, 2024

REFERENCES

1. Koga, S., Sekiya, H., Kondru, N., Ross, O.A., and Dickson, D.W. (2021). Neuropathology and molecular diagnosis of Synucleinopathies. Mol. Neurodegener. *16*, 83. https://doi.org/10.1186/s13024-021-00501-z.
2. Calabresi, P., Mechelli, A., Natale, G., Volpicelli-Daley, L., Di Lazzaro, G., and Ghiglieri, V. (2023). Alpha-synuclein in Parkinson's disease and other synucleinopathies: from overt neurodegeneration back to early synaptic dysfunction. Cell Death Dis. *14*, 176. https://doi.org/10.1038/s41419-023-05672-9.
3. Brás, I.C., and Outeiro, T.F. (2021). Alpha-synuclein: Mechanisms of release and pathology progression in synucleinopathies. Cells *10*, 1–19. https://doi.org/10.3390/cells10020375.
4. Lehtonen, Š., Sonninen, T.M., Wojciechowski, S., Goldsteins, G., and Koistinaho, J. (2019). Dysfunction of cellular proteostasis in Parkinson's disease. Front. Neurosci. *13*, 457. https://doi.org/10.3389/fnins.2019.00457.
5. Conway, K.A., Lee, S.J., Rochet, J.C., Ding, T.T., Harper, J.D., Williamson, R.E., and Lansbury, P.T., Jr. (2000). Accelerated oligomerization by Parkinson's disease linked α-synuclein mutants. Ann. N. Y. Acad. Sci. *920*, 42–45. https://doi.org/10.1111/j.1749-6632.2000.tb06903.x.
6. Kayed, R., Dettmer, U., and Lesné, S.E. (2020). Soluble endogenous oligomeric α-synuclein species in neurodegenerative diseases: Expression, spreading, and cross-talk. J. Parkinsons Dis. *10*, 791–818. https://doi.org/10.3233/JPD-201965.
7. Deger, J.M., Gerson, J.E., and Kayed, R. (2015). The interrelationship of proteasome impairment and oligomeric intermediates in neurodegeneration. Aging Cell *14*, 715–724. https://doi.org/10.1111/acel.12359.
8. Thibaudeau, T.A., Anderson, R.T., and Smith, D.M. (2018). A common mechanism of proteasome impairment by neurodegenerative disease-associated oligomers. Nat. Commun. *9*, 1097. https://doi.org/10.1038/s41467-018-03509-0.
9. Hipp, M.S., Park, S.H., and Hartl, F.U. (2014). Proteostasis impairment in protein-misfolding and -aggregation diseases. Trends Cell Biol. *24*, 506–514. https://doi.org/10.1016/j.tcb.2014.05.003.
10. Fouka, M., Mavroeidi, P., Tsaka, G., and Xilouri, M. (2020). In Search of Effective Treatments Targeting α-Synuclein Toxicity in Synucleinopathies: Pros and Cons. Front. Cell Dev. Biol. *8*, 559791. https://doi.org/10.3389/fcell.2020.559791.
11. Spillantini, M.G., Schmidt, M.L., Lee, V.M., Trojanowski, J.Q., Jakes, R., and Goedert, M. (1997). Alpha-synuclein in Lewy bodies. Nature *388*, 839–840. https://doi.org/10.1038/42166.
12. Fares, M.B., Jagannath, S., and Lashuel, H.A. (2021). Reverse engineering Lewy bodies: how far have we come and how far can we go? Nat. Rev. Neurosci. *22*, 111–131. https://doi.org/10.1038/s41583-020-00416-6.
13. Heras-Garvin, A., and Stefanova, N. (2020). MSA: From basic mechanisms to experimental therapeutics. Park. Relat. Disord. *73*, 94–104. https://doi.org/10.1016/j.parkreldis.2020.01.010.
14. Zhang, Y., Cao, H., and Liu, Z. (2015). Binding cavities and druggability of intrinsically disordered proteins. Protein Sci. *24*, 688–705. https://doi.org/10.1002/pro.2641.
15. Kumar, D., Sharma, N., and Giri, R. (2017). Therapeutic interventions of cancers using intrinsically disordered proteins as drug targets: C-myc as model system. Cancer Inform. *16*, 1176935117699408. https://doi.org/10.1177/1176935117699408.
16. Schweighauser, M., Shi, Y., Tarutani, A., Kametani, F., Murzin, A.G., Ghetti, B., Matsubara, T., Tomita, T., Ando, T., Hasegawa, K., et al. (2020). Structures of α-synuclein filaments from multiple system atrophy. Nature *585*, 464–469. https://doi.org/10.1038/s41586-020-2317-6.
17. Van der Perren, A., Gelders, G., Fenyi, A., Bousset, L., Brito, F., Peelaerts, W., Van den Haute, C., Gentleman, S., Melki, R., and Baekelandt, V. (2020). The structural differences between patient-derived α-synuclein strains dictate characteristics of Parkinson's disease, multiple system atrophy and dementia with Lewy bodies. Acta Neuropathol. *139*, 977–1000. https://doi.org/10.1007/s00401-020-02157-3.
18. Flagmeier, P., Meisl, G., Vendruscolo, M., Knowles, T.P.J., Dobson, C.M., Buell, A.K., and Galvagnion, C. (2016). Mutations associated with familial Parkinson's disease alter the initiation and amplification steps of α-synuclein aggregation. Proc. Natl. Acad.

Sci. USA *113*, 10328–10333. https://doi.org/10.1073/pnas.1604645113.

19. Prusiner, S.B., Woerman, A.L., Mordes, D.A., Watts, J.C., Rampersaud, R., Berry, D.B., Patel, S., Oehler, A., Lowe, J.K., Kravitz, S.N., et al. (2015). Evidence for α-synuclein prions causing multiple system atrophy in humans with parkinsonism. Proc. Natl. Acad. Sci. USA *112*, 5308–5317. https://doi.org/10.1073/pnas.1514475112.
20. Lee, H.J., Ricarte, D., Ortiz, D., and Lee, S.J. (2019). Models of multiple system atrophy. Exp. Mol. Med. *51*, 1–10. https://doi.org/10.1038/s12276-019-0346-8.
21. Shahnawaz, M., Mukherjee, A., Pritzkow, S., Mendez, N., Rabadia, P., Liu, X., Hu, B., Schmeichel, A., Singer, W., Wu, G., et al. (2020). Discriminating α-synuclein strains in Parkinson's disease and multiple system atrophy. Nature *578*, 273–277. https://doi.org/10.1038/s41586-020-1984-7.
22. Ferreira, N., Gram, H., Sorrentino, Z.A., Gregersen, E., Schmidt, S.I., Reimer, L., Betzer, C., Perez-Gozalbo, C., Beltoja, M., Nagaraj, M., et al. (2021). Multiple system atrophy-associated oligodendroglial protein p25α stimulates formation of novel α-synuclein strain with enhanced neurodegenerative potential. Acta Neuropathol. *142*, 87–115. https://doi.org/10.1007/s00401-021-02316-0.
23. Lehotzky, A., Oláh, J., Fekete, J.T., Szénási, T., Szabó, E., Győrffy, B., Várady, G., and Ovádi, J. (2021). Co-Transmission of Alpha-Synuclein and TPPP/p25 Inhibits Their Proteolytic Degradation in Human Cell Models. Front. Mol. Biosci. *8*, 666026. https://doi.org/10.3389/fmolb.2021.666026.
24. Stefanova, N. (2023). A Mouse Model of Multiple System Atrophy: Bench to Bedside. Neurotherapeutics *20*, 117–126. https://doi.org/10.1007/s13311-022-01287-8.
25. Mavroeidi, P., Arvanitaki, F., Karakitsou, A.K., Vetsi, M., Kloukina, I., Zweckstetter, M., Giller, K., Becker, S., Sorrentino, Z.A., Giasson, B.I., et al. (2019). Endogenous oligodendroglial alpha-synuclein and TPPP/p25α orchestrate alpha-synuclein pathology in experimental multiple system atrophy models. Acta Neuropathol. *138*, 415–441. https://doi.org/10.1007/s00401-019-02014-y.
26. Oláh, J., and Ovádi, J. (2014). Dual life of TPPP/p25 evolved in physiological and pathological conditions. Biochem. Soc. Trans. *42*, 1762–1767. https://doi.org/10.1042/BST20140257.
27. Ota, K., Obayashi, M., Ozaki, K., Ichinose, S., Kakita, A., Tada, M., Takahashi, H., Ando, N., Eishi, Y., Mizusawa, H., et al. (2014). Relocation of p25α/tubulin polymerization promoting protein from the nucleus to the perinuclear cytoplasm in the oligodendroglia of sporadic and COQ2 mutant multiple system atrophy. Acta Neuropathol. Commun. *2*, 136–154. https://doi.org/10.1186/s40478-014-0136-4.
28. Wong, J.H., Halliday, G.M., and Kim, W.S. (2014). Exploring Myelin Dysfunction in Multiple System Atrophy. Exp. Neurobiol. *23*, 337–344. https://doi.org/10.5607/en.2014.23.4.337.
29. Krejciova, Z., Carlson, G.A., Giles, K., and Prusiner, S.B. (2019). Replication of multiple system atrophy prions in primary astrocyte cultures from transgenic mice expressing human α-synuclein. Acta Neuropathol. Commun. *7*, 81. https://doi.org/10.1186/s40478-019-0703-9.
30. Watts, J.C., Giles, K., Oehler, A., Middleton, L., Dexter, D.T., Gentleman, S.M., DeArmond, S.J., and Prusiner, S.B. (2013). Transmission of multiple system atrophy prions to transgenic mice. Proc. Natl. Acad. Sci. USA *110*, 19555–19560. https://doi.org/10.1073/pnas.1318268110.
31. Mao, Y. (2021). Structure, Dynamics and Function of the 26S Proteasome. Subcell. Biochem. *96*, 1–151. https://doi.org/10.1007/978-3-030-58971-4_1.
32. Thibaudeau, T.A., and Smith, D.M. (2019). A practical review of proteasome pharmacology. Pharmacol. Rev. *71*, 170–197. https://doi.org/10.1124/pr.117.015370.
33. Sahu, I., and Glickman, M.H. (2021). Structural insights into substrate recognition and processing by the 20s proteasome. Biomolecules *11*, 148. https://doi.org/10.3390/biom11020148.
34. Finley, D., Chen, X., and Walters, K.J. (2016). Gates, Channels, and Switches: Elements of the Proteasome Machine. Trends Biochem. Sci. *41*, 77–93. https://doi.org/10.1016/j.tibs.2015.10.009.
35. Ben-Nissan, G., and Sharon, M. (2014). Regulating the 20S proteasome ubiquitin-independent degradation pathway. Biomolecules *4*, 862–884. https://doi.org/10.3390/biom4030862.
36. Fiolek, T.J., Magyar, C.L., Wall, T.J., Davies, S.B., Campbell, M.V., Savich, C.J., Tepe, J.J., and Mosey, R.A. (2021). Dihydroquinazolines enhance 20S proteasome activity and induce degradation of α-synuclein, an intrinsically disordered protein associated with neurodegeneration. Bioorg. Med. Chem. Lett. *36*, 127821. https://doi.org/10.1016/j.bmcl.2021.127821.
37. Fiolek, T.J., Keel, K.L., and Tepe, J.J. (2021). Fluspirilene Analogs Activate the 20S Proteasome and Overcome Proteasome Impairment by Intrinsically Disordered Protein Oligomers. Neuroscience *12*, 1438–1448. https://doi.org/10.1021/acschemneuro.1c00099.
38. Jones, C.L., Njomen, E., Sjögren, B., Dexheimer, T.S., and Tepe, J.J. (2017). Small Molecule Enhancement of 20S Proteasome Activity Targets Intrinsically Disordered Proteins. ACS Chem. Biol. *12*, 2240–2247. https://doi.org/10.1021/acschembio.7b00489.
39. Staerz, S.D., Jones, C.L., and Tepe, J.J. (2022). Design, Synthesis, and Biological Evaluation of Potent 20S Proteasome Activators for the Potential Treatment of α-Synucleinopathies. J. Med. Chem. *65*, 6631–6642. https://doi.org/10.1021/acs.jmedchem.1c02158.
40. Staerz, S.D., Lisabeth, E.M., Njomen, E., Dexheimer, T.S., Neubig, R.R., and Tepe, J.J. (2023). Development of a Cell-Based AlphaLISA Assay for High-Throughput Screening for Small Molecule Proteasome Modulators. ACS Omega *8*, 15650–15659. https://doi.org/10.1021/acsomega.3c01158.
41. Njomen, E., Osmulski, P.A., Jones, C.L., Gaczynska, M., and Tepe, J.J. (2018). Small Molecule Modulation of Proteasome Assembly. ACS Biochem. *57*, 4214–4224. https://doi.org/10.1021/acs.biochem.8b00579.
42. Trader, D.J., Simanski, S., Dickson, P., and Kodadek, T. (2017). Establishment of a suite of assays that support the discovery of proteasome stimulators. Biochim. Biophys. Acta. Gen. Subj. *1861*, 892–899. https://doi.org/10.1016/j.bbagen.2017.01.003.
43. Halder, S., Macatangay, N.J., Zerfas, B.L., Salazar-Chaparro, A.F., and Trader, D.J. (2022). Oleic amide derivatives as small molecule stimulators of the human proteasome's core particle. RSC Med. Chem. *13*, 1077–1081. https://doi.org/10.1039/d2md00133k.
44. Zhou, H., Shao, M., Guo, B., Li, C., Lu, Y., Yang, X., ShengnanLi, Li, H., Zhu, Q., Zhong, H., et al. (2019). Tetramethylpyrazine Analogue T-006 Promotes the Clearance of Alpha-synuclein by Enhancing Proteasome Activity in Parkinson's Disease Models. Neurotherapeutics *16*, 1225–1236. https://doi.org/10.1007/s13311-019-00759-8.
45. Osmulski, P.A., Karpowicz, P., Jankowska, E., Bohmann, J., Pickering, A.M., and Gaczyńska, M. (2020). New peptide-based pharmacophore activates 20S proteasome. Molecules *25*, 1439–1455. https://doi.org/10.3390/molecules25061439.
46. Opoku-Nsiah, K.A., de la Pena, A.H., Williams, S.K., Chopra, N., Sali, A., Lander, G.C., and Gestwicki, J.E. (2022). The YΦ motif defines the structure-activity relationships of human 20S proteasome activators. Nat. Commun. *13*, 1226. https://doi.org/10.1038/s41467-022-28864-x.
47. Gizyńska, M., Witkowska, J., Karpowicz, P., Rostankowski, R., Chocron, E.S., Pickering, A.M., Osmulski, P., Gaczynska, M., and Jankowska, E. (2019). Proline- and Arginine-Rich Peptides as Flexible Allosteric Modulators of Human Proteasome Activity. J. Med. Chem. *62*, 359–370. https://doi.org/10.1021/acs.jmedchem.8b01025.
48. Vanecek, A.S., Mojsilovic-Petrovic, J., Kalb, R.G., and Tepe, J.J. (2023). Enhanced Degradation of Mutant C9ORF72-Derived Toxic Dipeptide Repeat Proteins by 20S Proteasome Activation Results in Restoration of Proteostasis and Neuroprotection. ACS Chem. Neurosci. *14*, 1439–1448. https://doi.org/10.1021/acschemneuro.2c00732.
49. Njomen, E., Vanecek, A., Lansdell, T.A., Yang, Y.T., Schall, P.Z., Harris, C.M., Bernard, M.P., Isaac, D., Alkharabsheh, O., Al-Janadi, A., et al. (2022). Small Molecule 20S Proteasome Enhancer Regulates MYC Protein Stability and Exhibits Antitumor Activity in Multiple Myeloma. Biomedicines *10*, 938–954. https://doi.org/10.3390/biomedicines10050938.
50. Yeung, P.K., Hubbard, J.W., Korchinski, E.D., and Midha, K.K. (1993). Pharmacokinetics of chlorpromazine and key metabolites. Eur. J. Clin. Pharmacol. *45*, 563–569. https://doi.org/10.1007/BF00315316.
51. Yoshii, K., Kobayashi, K., Tsumuji, M., Tani, M., Shimada, N., and Chiba, K. (2000). Identification of human cytochrome P450 isoforms involved in the 7- hydroxylation of chlorpromazine by human liver microsomes. Life Sci. *67*, 175–184. https://doi.org/10.1016/S0024-3205(00)00613-5.
52. Eberhardt, J., Santos-Martins, D., Tillack, A.F., and Forli, S. (2021). AutoDock Vina 1.2.0: New Docking Methods, Expanded Force Field, and Python Bindings. J. Chem. Inf. Model. *61*, 3891–3898. https://doi.org/10.1021/acs.jcim.1c00203.
53. Trott, O., and Olson, A.J. (2010). AutoDock Vina: Improving the speed and accuracy of docking with a new scoring function, efficient optimization, and multithreading. J. Comput. Chem. *31*, 455–461. https://doi.org/10.1002/jcc.21334.
54. Zhou, P., Zou, J., Tian, F., and Shang, Z. (2009). Fluorine bonding -How does it work in protein-ligand interactions? J. Chem. Inf.

Model. *49*, 2344–2355. https://doi.org/10.1021/ci9002393.
55. Bauer, M.R., Jones, R.N., Baud, M.G.J., Wilcken, R., Boeckler, F.M., Fersht, A.R., Joerger, A.C., and Spencer, J. (2016). Harnessing Fluorine-Sulfur Contacts and Multipolar Interactions for the Design of p53 Mutant Y220C Rescue Drugs. ACS Chem. Biol. *11*, 2265–2274. https://doi.org/10.1021/acschembio.6b00315.
56. Bissantz, C., Kuhn, B., and Stahl, M. (2010). A medicinal chemist's guide to molecular interactions. J. Med. Chem. *53*, 5061–5084. https://doi.org/10.1021/jm100112j.
57. Mishizen-Eberz, A.J., Guttmann, R.P., Giasson, B.I., Day, G.A., Hodara, R., Ischiropoulos, H., Lee, V.M.Y., Trojanowski, J.Q., and Lynch, D.R. (2003). Distinct cleavage patterns of normal and pathologic forms of α-synuclein by calpain I *in vitro*. J. Neurochem. *86*, 836–847. https://doi.org/10.1046/j.1471-4159.2003.01878.x.
58. Goldbaum, O., Jensen, P.H., and Richter-Landsberg, C. (2008). The expression of tubulin polymerization promoting protein TPPP/p25alpha is developmentally regulated in cultured rat brain oligodendrocytes and affected by proteolytic stress. Glia *56*, 1736–1746. https://doi.org/10.1002/glia.20720.
59. Oláh, J., Szénási, T., Szunyogh, S., Szabó, A., Lehotzky, A., and Ovádi, J. (2017). Further evidence for microtubule-independent dimerization of TPPP/p25. Sci. Rep. *7*, 40594. https://doi.org/10.1038/srep40594.
60. Mavroeidi, P., Arvanitaki, F., Vetsi, M., Becker, S., Vlachakis, D., Jensen, P.H., Stefanis, L., and Xilouri, M. (2022). Autophagy mediates the clearance of oligodendroglial SNCA/alpha-synuclein and TPPP/p25A in multiple system atrophy models. Autophagy *18*, 2104–2133. https://doi.org/10.1080/15548627.2021.2016256.
61. Lindersson, E., Lundvig, D., Petersen, C., Madsen, P., Nyengaard, J.R., Højrup, P., Moos, T., Otzen, D., Gai, W.P., Blumbergs, P.C., et al. (2005). p25alpha Stimulates alpha-synuclein aggregation and is co-localized with aggregated alpha-synuclein in alpha-synucleinopathies. J. Biol. Chem. *280*, 5703–5715. https://doi.org/10.1074/jbc.M410409200.
62. Leestemaker, Y., de Jong, A., Witting, K.F., Penning, R., Schuurman, K., Rodenko, B., Zaal, E.A., van de Kooij, B., Laufer, S., Heck, A.J.R., et al. (2017). Proteasome Activation by Small Molecules. Cell Chem. Biol. *24*, 725–736.e7. https://doi.org/10.1016/j.chembiol.2017.05.010.
63. Li, J., Uversky, V.N., and Fink, A.L. (2001). Effect of familial Parkinson's disease point mutations A30P and A53T on the structural properties, aggregation, and fibrillation of human α-synuclein. Biochemistry *40*, 11604–11613. https://doi.org/10.1021/bi010616g.
64. Mauvezin, C., and Neufeld, T.P. (2015). Bafilomycin A1 disrupts autophagic flux by inhibiting both V-ATPase-dependent acidification and Ca-P60A/SERCA-dependent autophagosome-lysosome fusion. Autophagy *11*, 1437–1438. https://doi.org/10.1080/15548627.2015.1066957.
65. Lehotzky, A., Tirián, L., Tökési, N., Lénárt, P., Szabó, B., Kovács, J., and Ovádi, J. (2004). Dynamic targeting of microtubules by TPPP/p25 affects cell survival. J. Cell Sci. *117*, 6249–6259. https://doi.org/10.1242/jcs.01550.
66. Szénási, T., Oláh, J., Szabó, A., Szunyogh, S., Láng, A., Perczel, A., Lehotzky, A., Uversky, V.N., and Ovádi, J. (2017). Challenging drug target for Parkinson's disease: Pathological complex of the chameleon TPPP/p25 and alpha-synuclein proteins. Biochim. Biophys. Acta, Mol. Basis Dis. *1863*, 310–323. https://doi.org/10.1016/j.bbadis.2016.09.017.
67. Heravi, M., Dargahi, L., Parsafar, S., Tayaranian Marvian, A., Aliakbari, F., and Morshedi, D. (2019). The primary neuronal cells are more resistant than PC12 cells to α-synuclein toxic aggregates. Neurosci. Lett. *701*, 38–47. https://doi.org/10.1016/j.neulet.2019.01.055.
68. Gąssowska, M., Czapski, G.A., Pająk, B., Cieślik, M., Lenkiewicz, A.M., and Adamczyk, A. (2014). Extracellular α-synuclein leads to microtubule destabilization via GSK-3β-dependent tau phosphorylation in PC12 cells. PLoS One *9*, 94259. https://doi.org/10.1371/journal.pone.0094259.
69. Ejlerskov, P., Rasmussen, I., Nielsen, T.T., Bergström, A.L., Tohyama, Y., Jensen, P.H., and Vilhardt, F. (2013). Tubulin polymerization-promoting protein (TPPP/p25α) promotes unconventional secretion of α-synuclein through exophagy by impairing autophagosome-lysosome fusion. J. Biol. Chem. *288*, 17313–17335. https://doi.org/10.1074/jbc.M112.401174.
70. Gaur, P., Galkin, M., Kurochka, A., Ghosh, S., Yushchenko, D.A., and Shvadchak, V.V. (2021). Fluorescent Probe for Selective Imaging of α-Synuclein Fibrils in Living Cells. ACS Chem. Neurosci. *12*, 1293–1298. https://doi.org/10.1021/acschemneuro.1c00090.
71. Hasegawa, T., Baba, T., Kobayashi, M., Konno, M., Sugeno, N., Kikuchi, A., Itoyama, Y., and Takeda, A. (2010). Role of TPPP/p25 on α-synuclein-mediated oligodendroglial degeneration and the protective effect of SIRT2 inhibition in a cellular model of multiple system atrophy. Neurochem. Int. *57*, 857–866. https://doi.org/10.1016/j.neuint.2010.09.002.
72. Zotter, Á., Bodor, A., Oláh, J., Hlavanda, E., Orosz, F., Perczel, A., and Ovádi, J. (2011). Disordered TPPP/p25 binds GTP and displays Mg2+-dependent GTPase activity. FEBS Lett. *585*, 803–808. https://doi.org/10.1016/j.febslet.2011.02.006.
73. Orosz, F. (2012). A New Protein Superfamily: TPPP-Like Proteins. PLoS One *7*, 49276. https://doi.org/10.1371/journal.pone.0049276.

STAR★METHODS

KEY RESOURCES TABLE

REAGENT or RESOURCE	SOURCE	IDENTIFIER
Antibodies		
Mouse Monoclonal Anti-α-synuclein	Novus Biologics	NBP2-15365
Rabbit Monoclonal Anti-p25α	Novus Biologics	NBP1-91613
Mouse HRP Tagged Anti-GAPDH	Novus Biologics	NBP2-27103H
Anti-Rabbit HRP-Linked	Cell Signaling	7074S
Anti-Mouse HRP-Linked	Cell Signaling	70745
Rabbit Anti-α-synuclein	Abcam	ab212184
Mouse HRP Tagged Anti-Ubiquitin	Santa Cruz	sc-8017
Recombinant DNA		
Human Tppp cDNA Clone	genomics online	ABIN4629840
Tubulin Polymerization Promoting Protein (TPPP) (NM_007030) Human Tagged ORF Clone	Origene	RC213142
pHM6-α-synuclein-A53T	Addgene	40825
Chemicals, peptides and recombinant proteins		
Human 20S Proteasome Protein, CF	R&D Systems	E-360-050
Suc-Leu-Leu-Val-Tyr-AMC (Suc-LLVY-AMC)	R&D Systems	S-280-05M
Z-Leu-Leu-Glu-AMC (Z-LLE-AMC)	Cayman Chemicals	10008117
Boc-LRR-AMC (trifluoroacetate salt)	Cayman Chemicals	26642
Recombinant Human alpha-synuclein Protein, CF	R&D Systems	SP-485-500
Recombinant Human GAPDH Protein	R&D Systems	NBP2-52615
Dulbecco's Modified Eagle's Medium	Gibco	11995-065
Penicillin–Streptomycin	Gibco	15140-122
Fetal Bovine Serum	Gibco	26140-079
RPMI 1640	Gibco	11875-093
Horse Serum Donor Herd	Sigma-Aldrich	H1270
Opti-mem	Gibco	31985-070Ch
SOC Medium	Sigma-Aldrich	S1797
Kanamycin sulfate from Streptomyces kanamyceticus	Sigma-Aldrich	K1377
Lysogeny broth	Neogen	NGM0088A
IPTG	Sigma-Aldrich	I6758
cOmplete™, Mini, EDTA-free Protease Inhibitor Cocktail	Sigma-Aldrich	11836170001
Xtreme gene	Sigma-Aldrich	6366236001
PBS	Sigma-Aldrich	D8537
RIPA Buffer	Sigma-Aldrich	R0278
Pierce BCA Protein Analysis Kit	ThermoFisher Scientific	23225
Laemmli Sample Buffer	Bio-Rad	1610747
2-Mercaptoethanol	Sigma-Aldrich	M6250
4-20% Tris-glycine SDS-PAGE gel	Bio-Rad	4561096
PVDF membrane	Bio-Rad	1620177
Blotting Grade Blocker	Bio-Rad	1706404
Radiance plus	Azure Biosystems	AC2103

(*Continued on next page*)

Continued

REAGENT or RESOURCE	SOURCE	IDENTIFIER
Me4BodipyFL-Ahx3Leu3VS Fluorescent probe	R&D Systems	I-190
RP1 Probe	Gaur, P.; et al.[70]	N/A
Proteasome Glo Reagent	Promega	G8660
Cell Titer Glo Reagent	Promega	G3580
TCH-165	Njomen, E.; et al.[41]	N/A
Bortezomib	Cayman Chemicals	10008822
HisTrap HP His tag protein purification columns	Cytiva	29051021
Amicron ultra-15 10 K filters	Millipore Sigma	UFC901008
Flowmi® Cell Strainers (with a porosity of 40 μm)	Sigma-Aldrich	BAH136800040
Experimental models: Cell lines		
HEK-293T	ATCC	CRL-3216
PC-12	ATCC	CRL-1721
Experimental models: Organisms/strains		
E. Coli BL21(DE3)	ThermoFisher Scientific	EC0114
Software and algorithms		
Bio-Rad Image Lab software	Bio-Rad	Bio-Rad: https://www.bio-rad.com/en-us/product/image-lab-software?ID=KRE6P5E8Z
GraphPad Prism 8	GraphPad	GraphPad: https://www.graphpad.com/scientific-software/prism/
Softmax Pro 7.1	Molecular Devices	Molecular Devices: https://support.moleculardevices.com/s/article/SoftMax-Pro-7-1-software-Download-page

RESOURCE AVAILABILITY

Lead contact

Further information and requests for resources and reagents should be directed to and will be fulfilled by the lead contact, Dr. Jetze Tepe (tepe@virginia.edu).

Materials availability

All unique/stable reagents generated in this study are available from the lead contact without restriction.

Data and code availability

- This paper does not report original code.
- All data reported in this paper will be shared by the lead contact upon request.
- Any additional information required to reanalyze the data reported in this paper is available from the lead contact upon request.

EXPERIMENTAL MODEL AND STUDY PARTICIPANT DETAILS

Mammalian cell line

HEK-293T and PC12 cells were purchased from American Type Culture Collection (ATCC) and all plasmids used to transfect these cell lines were purchased.

Bacteria cell culture

In vitro experiments using TPPP/p25α were performed with recombinant protein purified from electro-competent *E.Coli* (BL21 DE3) cells expressing TPPP/p25α.

METHOD DETAILS

Cell culture

HEK-293T cells were cultured in Dulbecco's modified Eagle's medium supplemented with 1% penicillin–streptomycin and 10% fetal bovine serum. PC12 cells were cultured in RPMI 1640 supplemented with 1% penicillin–streptomycin, 5% fetal bovine serum and 10% horse serum. All cell lines were maintained at 37°C with 5% CO_2 in 10 cm tissue treated plates. Cell lines were routinely tested for mycoplasma contamination.

Antibodies

Primary antibodies used for the immunoblotting of the purified α-synuclein degradation, *in vitro* proteasome impairment, and the HEK-293T cellular studies were mouse monoclonal anti-α-synuclein IgG (1:1333) and anti-mouse HRP-linked IgG (1:1000). For the *in vitro* degradation of p25α, rabbit monoclonal anti-p25α IgG (1:1000) and anti-rabbit HRP-linked IgG (1:1000), were used. The PC12 cellular studies utilized rabbit anti-α-synuclein IgG (1:1000) and HRP tagged anti-ubiquitin (1:1000). For all studies the HRP tagged anti-GAPDH (1:1333) was used.

Protein purification

The Human Tppp cDNA Clone was transformed into *E. Coli* BL21(DE3) strains, 10 ng/μL of plasmid was added to 50 μL of electro-competent *E. Coli* BL21(DE3). The sample was then transferred to an ice cold, sterile Gene Pulser electroporation cuvette, and pulsed at 2.5 kV (25 mF capacitance, 200 Ω resistance) using a Bio-Rad Gene Pulser II electroporation system. Cells were immediately resuspended in 1 mL of SOC and the resulting mixture was shaken at 37°C for 1 hour at 300 rpm. After that, the cells were spread on LB agar plate containing 50 mg/mL kanamycin overnight at 37°C.

A 5 mL of LB media in a falcon tube was supplemented with 50 mg/mL kanamycin was inoculated with a single colony of *E. Coli* BL21(DE3)/pPB transformant and the cultures were shaken at 37°C overnight at 300 rpm. The overnight cultures were used to inoculate a 1 L flask of LB media containing 50 mg/mL kanamycin to an Optical Density (OD_{600}) of 0.05. At an OD_{600} of 0.6-0.7, protein expression was induced with 0.05 mM IPTG. The culture was shaken at 40°C for 8 hours. The cells were pelleted by centrifuging (12000 rpm, 4°C, 15 minutes) and pellets were stored at -20°C before purification.

Cell pellets were thawed and suspended in lysis buffer containing 20 mM sodium phosphate, pH 7.2, 2.0 mM imidazole, 500 mM sodium chloride, and protease inhibitor cocktail (2 mL of lysis buffer/gram of cell paste). Cells were lysed by two passes through French Pressure Cell at 18,000 psi. The lysate was centrifuged (20000 rpm, 4°C, 30 minutes) and the supernatant was filtered through a 0.45 μm sterile syringe filter. The crude lysate was then applied to a HisTrap FF 1 mL nickel affinity column and purified on an ÄKTA Start FPLC system. The equilibration buffer contained 20 mM sodium phosphate, pH 7.2, 2.0 mM imidazole, and 500 mM sodium chloride, and elution was done with 20 mM sodium phosphate, pH 7.2, 2.0 mM imidazole, 500 mM sodium chloride with an imidazole gradient of 20 mM to 500 mM. 20 column volumes of elution buffer were used in total. The fractions containing purified protein were pooled, concentrated using Amicron ultra-15 10 K filters, and stored in 100 mM sodium phosphate pH 8.0 with 20% ethylene glycol.

Transfection and immunoblotting

The HEK-293T cells were plated in 60 mm plates and grown to 80% confluency. The cells were then transiently transfected with Xtreme gene and the desired plasmid (5 μg of DNA, TPPP and A53T α-synuclein, and 10 μL of transfection reagent for a 1:2 dilution) diluted in 500 μL Opti-mem. The expression of the target protein was conducted for 48 hours before treatment for an additional 16 hours. After the cells were treated with the test compounds or DMSO, the cells were scraped from the plate and washed with PBS. The plate was washed with PBS as well. The scraped cells in media and PBS were pelleted (300g for 5 minutes). The supernatant was removed, and the cell pellet was washed with ice cold PBS and once again pelleted (300g for 5 minutes). The PBS supernatant was removed, and the cell pellet was lysed with RIPA buffer with added protease inhibitors. The cell lysate was incubated for 15 minutes on ice. The lysate was centrifuged for 25 minutes at 500 g, then the supernatant was removed while the debris pellet was disposed of.

Like the experiments with the HEK-293T cells, the PC12 were plated in 60 mm plates after being strained with Flowmi® Cell Strainers. The PC12 cells were then transfected in the same manner as the HEK-293T cells, using the same protein expression and treatment period. After the treatments, the cells were collected with media and pelleted (300g for 5 minutes). The supernatant was removed, and the cell pellet was washed with ice cold PBS and pelleted again (300g for 5 minutes). The PBS supernatant was removed, and the cell pellet was resuspended with PBS that contained protease inhibitors and lysed using sonication. The lysate was centrifuged for 25 minutes at 1000 g, then the supernatant was removed while the debris pellet was disposed. The concentration of total protein in each sample was calculated using the Pierce BCA Protein Analysis Kit, and lysates were standardized to the lowest total protein concentration.

For all immunoblotting, a concentrated Laemmli sample buffer supplemented with 25% β-mercaptoethanol was added to all the samples and boiled for 10 minutes. The samples were then resolved on a 4-20% Tris-glycine SDS-PAGE gel and transferred onto a PVDF membrane using Mini Trans-Blot Electrophoretic Transfer Cell for 1 hour and 30 minutes. The membranes were blocked for 30 minutes with 5% Blocking Buffer at room temperature. The membrane was then incubated with the desired primary antibody (listed in the antibody section with dilution ratios) in 10 mL of Tris-buffered saline Tween 20 (TBST: 1x solution was made from a 10x TBS solution) at 4°C for 16 hours. The immunoblots were washed with 1x TBST for 3x3 minutes before being incubated with the corresponding secondary antibody at room temperature for 1 hour. The immunoblots were developed with ECL Western reagent and imaged with an Azure Biosystems 300Q imager. If several proteins were probed for, the immunoblots were stripped using a mild stripping buffer (200 mM glycine, 3.5 mM SDS, and 8 mM Tween 20 with a pH of

2.2) for 20 minutes and then washed with TBST for 3x 5 minutes before re-probing. Immunoblots were then quantified using the Bio-Rad Image Lab software.

Fluorogenic small peptide assay with purified 20S proteasome

The purified enzymatic activity assays were carried out in a black flat/clear bottom 96-well plate with a reaction volume of 100 μL. Different concentrations (3.75−30 μM or 0.16−30 μM) of test compounds were added to the wells containing 0.5 nM of human constitutive 20S proteasome diluted in a 38 mM Tris and 100 mM NaCl buffer with a pH of 7.8. The drug:proteasome mixture was incubated for 20 minutes at 37°C. Then, 10 μL of the fluorogenic substrates were added. The fluorogenic substrates used were a combination of Suc-LLVY-AMC, Z-LLE-AMC, and Boc-LRR-AMC with a final concentration of 6.67 μM of each. The activity was measured at 37°C on a SpectraMax M5e spectrometer by measuring the change in fluorescence unit per minute for one hour at 380/460 nm. The rate of hydrolysis for the vehicle control was set at 100%, and the ratio of the treated sample over the vehicle control was used to calculate the fold change in rate of substrate hydrolysis by the proteasome.

Purified α-synuclein digestion with 20S proteasome

Proteolytic digestions of α-synuclein assays were carried out in a 25 μL reaction volume of 50 mM HEPES and 5 mM DTT buffer at a pH of 7.2, 300 nM of purified α-synuclein, and 10 nM purified human 20S proteasome. The 20S proteasome was first diluted to 11.1 nM in the HEPES buffer, and 0.5 μL of the test compounds in DMSO or DMSO alone were added. The drug:proteasome solution was incubated for 45 minutes at 37°C. After this incubation, 2.5 μL of a 3 μM stock of α-synuclein was added, and the mixture was incubated at 37°C for an additional 3.5 hours. After the second incubation, 0.5 μM of GAPDH was added as a loading control. A concentrated SDS loading buffer was also added, then the samples were boiled for 15 minutes to stop the digestion and immunoblotted.

Purified p25α digestion with 20S proteasome

The degradation of p25α was carried out in a total reaction volume of 25 μL. A solution of an 8.5 nM proteasome stock was made in 120 mM NaCl, 50 mM Tris, and 0.1% β-mercaptoethanol buffer with a pH of 7.2. A final concentration of 7.5 nM of 20S proteasome was treated with 0.5 μL of either DMSO or 10 μM of **1**, **4**, or **19** for 30 minutes at 37°C. During this 30-minute incubation, a 5,000 nM stock of purified p25α was incubated with 100 μM of DTE for 30 minutes at room temperature. After incubation, the purified 2.5 μL p25α (final concentration of 500 nM) was added to the drug:proteasome solution for an additional 3 hours. Then, 0.5 μM of GAPDH was added as a loading control. A concentrated SDS loading buffer was also added, then the samples were boiled for 15 minutes to stop the digestion and immunoblotted.

Purified 20S proteasome impairment by p25α/α-synuclein aggregates

Proteasome impairment was evaluated in a 50 μL reaction volume, and a stock solution of 18.75 nM of 20S proteasome was made in a 120 mM NaCl, 50 mM Tris, and 0.1% β-mercaptoethanol buffer with a pH of 7.2. Samples were then made with 40 μL of a 20S proteasome solution (final concentration of 15 nM) and then 5 μL of either PBS, α-synuclein (final concentration of 700 nM), or p25α (final concentration of 150 nM) for 45 minutes at 37°C. An additional sample of 700 nM α-synuclein and 150 nM p25α were incubated for 45 minutes at 37°C. After this incubation, 1 μL of Me4BodipyFL-Ahx3Leu3VS fluorescent probe was added to a final concentration of 1.5 μM. Then, 0.5 μM of GAPDH was added as a loading control. A concentrated SDS loading buffer was also added, then the samples were boiled for 15 minutes to stop the digestion. The samples were then resolved on a 4-20% Tris-glycine SDS-PAGE gel, and the fluorescence was visualized using Azure Biosystems 300Q imager at an excitation of 524 nm and emission of 572 nm. The samples were then immunoblotted.

P25α induced α-synuclein fibrillization and proteasome impairment in PC12 cells

The PC12 cells transiently transfected with the A53T α-synuclein plasmid were treated with either DMSO or 10 μM of compounds **1**, **4**, or **19** for 2 hours, or cells were treated with purified p25α (final concentration of 160 nM, diluted in PBS) for 2 hours (after the 48-hour expression period). After this incubation, the cells treated with the compounds first were treated with purified p25α. The cells treated with p25α first were then treated with DMSO or 10 μM of compounds **1**, **4**, or **19** (0.1 % final DMSO concentration). After this second treatment, cells were incubated for an additional 24 hours.

RB1 probe fibrillization

Prior to being lysed, PC12 cells were once again strained with the tip cell strainer and plated to 10,000 cells/well (100 μL volume) in a black opaque bottom 96-well plate. Then, 1 μL of the RB1 probe (final concentration of 800 nM, synthesized following reported protocol)[64] were added to each plate and incubated for 45 minutes at 37°C. After this incubation, the fluorescence of each well was evaluated using a microplate reader at an excitation of 561 nm and emission of 589 nm.

Proteasome Glo

Like the RB1 probe assay, prior to lysis, the PC12 cells were strained and plated to 3,000 cells/well in a white 384-well plate at a 20 μL volume. Then, 10 μL of the Proteasome Glo reagent was added and incubated at room temperature for 20 minutes. The luminescence for each well was identified using the microplate reader.

Cytotoxicity

The PC12 cells were plated in a white 384-well plate (2,500 cells/well at a 15 μL total volume) after being strained with a cell strainer. Each well was either transfected with no plasmid, 0.5 μg of an A53T α-synuclein plasmid, 0.1 μg of a p25α plasmid, or a combination of the A53T α-synuclein and p25α plasmids and 1.2 μL of the transfection reagent (diluted in a final volume of 15 μL in the Opti-mem). After a 24-hour transfection, DMSO and 3 μM of **1**, **4**, and **19** were added (DMSO samples of each treatment were diluted in Opti-mem to a final DMSO concentration of 0.03%) for an additional 72 hours. Then, 10 μL of the Cell Titer Glo reagent or 10 μL of the Proteasome Glo reagent were added, and the luminescence per well was recorded. The cell viability and proteasome activity assays for the HEK-293T cells were conducted in the same manner, but with the following alterations. The A53T α-synuclein plasmid was lowered to 0.1 μg with 0.02 μg of the p25α plasmid. The treatment time was lowered to 48 hours from 72 hours.

Systematic treatment with purified p25α

PC12 cells were plated at 2,500 cells/well in a white 384-well plate to a volume of 15 μL. Cells were then transfected with either no plasmid or 0.5 μg of the A53T α-synuclein plasmid and 1 μL of the transfection reagent (diluted up to 15 μL of Opti-mem). After 24 hours, cells were treated with DMSO or 3 μM of compounds **1**, **4**, and **19**. The cells were also treated with 160 nM of p25α, which was done every 24 hours for 3 days. Then, 10 μL of the Cell Titer Glo reagent was added, and the luminescence per well was recorded.

Chemistry

General acylation procedure

The bis(fluorophenyl) amine (1.0 equiv) and TEA (1.3 equiv) were dissolved in DCM (15.0 mL) and cooled to 0°C, and the desired acyl halide (1.2 equiv) was added dropwise. The reaction mixture was warmed to room temperature and left to stir for 12 hours under inert N_2 gas. The crude reaction was washed with brine (2 x 10 mL) and extracted with DCM (2 x 10 mL). The organic layer was dried over anhydrous Na_2SO_4, filtered, and concentrated under reduced pressure. The desired product was purified using an automated CombiFlash chromatography (silica gel, 20-40 microns, 20−40 μm, with a gradient mobile phase of 0% - 40% EtOAc in Hexane).

General procedure A

The desired heterocycle (1.0 equiv) was dissolved in DMF (3.0 mL) and cooled to 0°C. Then, NaH (1.1 equiv) was added, and the mixture stirred at 0°C for one hour. The corresponding *N,N*-bis(4-fluorophenyl) amide (2 equiv) was added, and the reaction was slowly warmed to room temperature and stirred for 24 hours under inert N_2 gas. The crude mixture was washed with LiBr (3 x 9 mL), and the organic layer was extracted with EtOAc (1 x 10 mL). The organic layer was dried over anhydrous Na_2SO_4, filtered, concentrated under reduced pressure, and purified using an automated CombiFlash chromatography (silica gel, 20−40 μm, with a gradient mobile phase of 0% - 20% EtOAc in Hexane).

General procedure B

The desired heterocycle (1.0 equiv) and the corresponding N, N-bis(4-fluorophenyl) amide (1.0 equiv) were dissolved in toluene (5.0 mL). Then, TEA (4.0 equiv) was added dropwise, and the solution was refluxed for 24 hours under inert N_2 gas. The crude mixture was washed with brine (3 x 5 mL), and the organic layer was extracted with DCM (1 x 10 mL). The organic layer was dried over anhydrous Na_2SO_4, filtered, concentrated under reduced pressure, and purified using an automated CombiFlash chromatography (silica gel, 20−40 μm, with a gradient mobile phase of 0% - 20% EtOAc in Hexane).

General procedure C

The corresponding *N,N*-bis(4-fluorophenyl) amide (1.0 equiv) was dissolved in THF (5 mL), and TEA (1.2 equiv) was added dropwise. Then, 2 M dimethyl amine in THF (2.0 equiv) was added dropwise, and the solution stirred for 24 hours at room temperature under inert N_2 gas. The crude mixture was washed with brine (3 x 5 mL), and the organic layer was extracted with DCM (10 mL). The crude mixture was dried over Na_2SO_4, filtered, concentrated under reduced pressure, and purified using an automated CombiFlash chromatography (silica gel, 20−40 μm, with a gradient mobile phase of 0 - 30% EtOAc in Hexane).

2-chloro-N,N-bis(4-fluorophenyl)acetamide (S1)

General acylation procedure produced a light-yellow solid (67%). MP: 95-97°C. ^{1}H NMR (CD_2Cl_2, 500 MHz) δ 7.34-7.10 (m, 8H), 4.05 (s, 2H). ^{13}C{^{1}H} NMR (DMSO-d_6, 126 MHz) δ 166.0, 139.2, 138.2, 131.4, 129.3, 117.2, 116.3, 43.7. IR: 3067 cm^{-1}, 2980 cm^{-1}, 1686 cm^{-1}, 1503 cm^{-1}. HRMS (APCI) *m/z*: [M+H]+ calc'd for ($C_{14}H_{11}ClF_2NO^+$) 282.0492; Found 282.0338. *^{1}H NMR and ^{13}C{^{1}H} NMR were run in different solvents for better resolution of the observed peaks.

3-bromo-N,N-bis(4-fluorophenyl)propanamide (S2)

General acylation procedure produced a pale pink solid (88%). MP: 94-96°C. ^{1}H NMR ($CDCl_3$, 500 MHz) δ 7.22-7.03 (m, 8H), 3.66 (t, *J* = 6.6 Hz, 2H), 2.82 (t, *J* = 6.6 Hz, 2H). ^{13}C{^{1}H} NMR ($CDCl_3$, 126 MHz) δ 170.1, 138.1 138.13, 138.11, 130.3, 127.9, 117.2, 116.0, 37.9, 27.5. IR: 3117 cm^{-1}, 2950 cm^{-1}, 1600 cm^{-1}, 1425 cm^{-1}. HRMS (APCI) *m/z*: [M+H]+ calc'd for ($C_{15}H_{13}BrF_2NO^+$) 340.0143; Found 340.0063.

3-(9H-carbazol-9-yl)-N,N-bis(4-fluorophenyl)propanamide (1)

General procedure A produced a white solid (59%). MP:177-178°C. ^{1}H NMR (DMSO-d_6, 500 MHz) δ 8.16 (d, J = 8.0 Hz, 2H), 7.48 (dt, J = 8.0, 0.9 Hz, 2H), 7.42-7.38 (m, 2H), 7.22-7.18 (m, 2H), 7.12 (t, J = 8.4 Hz, 2H), 7.07-7.05 (m, 4H), 6.97 (t, J = 8.1 Hz, 2H), 4.66 (t, J = 6.9 Hz, 2H), 2.65 (t, J = 6.9 Hz, 2H). ^{13}C{^{1}H} NMR ($CDCl_3$, 126 MHz) δ 171.3, 139.9, 137.99, 137.96, 129.6 (d, J = 8.6 Hz), 128.1 (d, J = 8.4 Hz), 125.9, 122.9, 120.3, 119.3, 116.5 (d, J = 22.6 Hz), 115.9 (d, J = 22.9 Hz), 109.0, 40.0, 33.3. IR: 3059 cm^{-1}, 2992 cm^{-1}, 1659 cm^{-1}, 1327 cm^{-1}. HRMS (APCI) *m/z*: [M+H]+ calc'd for ($C_{27}H_{21}F_2N_2O^+$) 427.1616; Found 427.1641. *^{1}H NMR and ^{13}C{^{1}H} NMR were run in different solvents for better resolution of the observed peaks.

2-(9H-carbazol-9-yl)-N,N-bis(4-fluorophenyl)acetamide (2)

General Procedure A produced a white solid (92%). MP: 189-190°C. ^{1}H NMR ($CDCl_3$, 500 MHz) δ 8.05 (d, J = 7.7 Hz, 2H), 7.41 (t, J = 7.7 Hz, 2H), 7.26-7.20 (m, 4H), 7.15-6.93 (m, 8H), 5.01 (s, 2H). ^{13}C{^{1}H} NMR ($CDCl_3$, 126 MHz) δ 168.0, 140.2, 138.3, 136.9, 129.4, 127.5, 125.7, 123.1, 120.3, 119.6, 117.1, 115.9, 108.3, 46.8. IR: 3069 cm^{-1}, 2978 cm^{-1}, 1668 cm^{-1}, 1501 cm^{-1}. (APCI) m/z: [M+H]+ calc'd for ($C_{26}H_{19}F_2N_2O^+$) 413.1460; Found 413.1466.

3-(2-chloro-9H-carbazol-9-yl)-N,N-bis(4-fluorophenyl)propanamide (3)

General procedure A produced a white solid in 88% yield. MP: 133-134°C. ^{1}H NMR (DMSO-d_6, 500 MHz) δ 8.17 (dd, J = 8.1, 1.5 Hz, 2H), 7.57 (d, J = 1.8 Hz, 1H), 7.51 (d, J = 8.2 Hz, 1H), 7.45-7.42 (m, 1H), 7.25-7.20 (m, 2H), 7.14-7.00 (m, 8H), 4.64 (t, J = 6.8 Hz, 2H), 2.66 (t, J = 6.8 Hz, 2H).^{13}C{^{1}H} NMR ($CDCl_3$, 126 MHz) δ 171.0, 140.4, 140.3, 137.92, 137.89, 131.7, 129.6 (d, J = 8.6 Hz), 128.0 (d, J = 8.8 Hz), 126.2, 122.3, 121.5, 121.2, 120.3, 119.9, 119.8, 116.6 (d, J = 22.8 Hz), 116.0 (d, J = 22.5 Hz), 109.2, 109.0, 40.0, 33.3. IR: 3030 cm^{-1}, 2865 cm^{-1}, 1605 cm^{-1}, 1320 cm^{-1}. HRMS (APCI) *m/z*: [M+H]+ calc'd for ($C_{27}H_{20}ClF_2N_2O^+$) 462.1227; Found 462.1157. *^{1}H NMR and ^{13}C{^{1}H} NMR were run in different solvents for better resolution of the observed peaks.

N,N-bis(4-fluorophenyl)-2-(2-methyl-9H-carbazol-9-yl)acetamide (4)

General procedure A produced a light-yellow solid (58%). MP: 129-130°C ^{1}H NMR ($CDCl_3$, 500 MHz) δ 8.00 (dd, J = 8.1, 1.2 Hz, 1H), 7.91 (d, J = 8.2 Hz, 1H), 7.45-7.42 (m, 1H), 7.27-7.24 (m, 2H), 7.19 (dd, J = 8.2, 1.8 Hz, 1H), 7.16-7.09 (m, 5H), 6.97 (t, J = 8.3 Hz, 4H), 4.92 (s, 2H). ^{13}C{^{1}H} NMR ($CDCl_3$, 126 MHz) δ 167.4, 140.8, 140.6, 138.0, 136.8, 131.5, 129.5, 127.4, 126.1, 122.6, 121.7, 121.1, 120.3, 120.2, 120.0, 117.4 (d, J = 22.5 Hz), 116.0 (d, J = 22.8 Hz), 108.7, 108.6, 46.7. IR: 3057 cm^{-1}, 2960 cm^{-1}, 1670 cm^{-1}, 1280 cm^{-1}. HRMS (APCI) *m/z*: [M+H]+ calc'd for ($C_{26}H_{18}ClF_2N_2O^+$) 447.1070; Found 447.1142.

N,N-bis(4-fluorophenyl)-3-(9H-pyrido[3,4-b]indol-9-yl)propanamide (5)

General procedure A produced a light-yellow solid in 38% yield. MP: 192-193°C. ^{1}H NMR ($CDCl_3$, 500 MHz) δ 8.82 (s, 1H), 8.51 (s, 1H), 8.19 (dt, J = 7.9, 1.0 Hz, 1H), 8.00 (d, J = 5.0 Hz, 1H), 7.61-7.58 (m, 1H), 7.50-7.48 (m, 1H), 7.35-7.32 (m, 1H), 6.94-6.74 (m, 6H), 6.62 (dd, J = 8.7, 4.7 Hz, 2H), 4.81 (t, J = 6.5 Hz, 2H), 2.83 (t, J = 6.5 Hz, 2H).^{13}C{^{1}H} NMR ($CDCl_3$, 126 MHz) δ 170.7, 140.9, 139.2, 137.8, 132.8, 132.1, 129.6 (d, J = 8.5 Hz), 128.7, 127.9 (d, J = 8.7 Hz), 121.9, 121.2, 121.1, 120.3, 120.1, 116.8 (d, J = 22.7 Hz), 116.0 (d, J = 22.7 Hz), 111.9, 109.9, 40.1, 33.7. IR: 3078 cm^{-1}, 2895 cm^{-1}, 1620 cm^{-1}, 1355 cm^{-1}. HRMS (APCI) *m/z*: [M+H]+ calc'd for ($C_{26}H_{20}F_2N_3O^+$) 428.1569; Found 428.1480.

N,N-bis(4-fluorophenyl)-2-(9H-pyrido[3,4-b]indol-9-yl)acetamide (6)

General procedure A produced a light-yellow solid (65%). MP:161-162°C. ^{1}H NMR ($CDCl_3$, 500 MHz) δ 8.76 (s, 1H), 8.44 (d, J = 5.3 Hz, 1H), 8.12 (dt, J = 7.9, 1.0 Hz, 1H), 7.94-7.93 (m, 1H), 7.60-7.57 (m, 1H), 7.36 (dt, J = 8.3, 0.9 Hz, 1H), 7.33-7.29 (m, 1H), 7.24-7.18 (m, 8H), 5.08 (s, 2H). ^{13}C{^{1}H} NMR ($CDCl_3$, 126 MHz) δ 166.9, 141.5, 138.6, 137.8, 136.8, 136.4, 131.0, 129.7, 129.3, 128.9, 127.5, 122.1, 121.3, 120.6, 117.6 (d, J = 22.5 Hz), 116.0 (d, J = 22.5 Hz), 114.7, 109.3, 46.6. IR: 3062 cm^{-1}, 2954 cm^{-1}, 1686 cm^{-1}, 1450 cm^{-1}. HRMS (APCI) *m/z*: [M+H]+ calc'd for ($C_{25}H_{18}F_2N_3O^+$) 414.1412; Found 414.1446.

N,N-bis(4-fluorophenyl)-3-(1H-indol-1-yl)propanamide (7)

General procedure A produced a white waxy solid in 65% yield. ^{1}H NMR ($CDCl_3$, 500 MHz) δ 7.68-7.66 (m, 1H), 7.18-7.12 (m, 4H), 7.06-6.97 (m, 4H), 6.77 (t, J = 8.2 Hz, 2H), 6.58 (dd, J = 8.6, 4.8 Hz, 2H), 6.53 (d, J = 3.1 Hz, 1H), 4.54 (t, J = 6.2 Hz, 2H), 2.70 (t, J = 6.2 Hz, 2H). ^{13}C{^{1}H} NMR ($CDCl_3$, 126 MHz) δ 171.0, 138.1, 138.0, 135.6, 129.9 (d, J = 8.6 Hz), 128.7, 128.6, 128.1 (d, J = 8.5 Hz), 121.7, 121.1, 119.6, 116.7 (d, J = 22.9 Hz), 116.0 (d, J = 22.6 Hz), 109.3, 101.4, 43.1, 35.0. IR: 3107 cm^{-1}, 2970 cm^{-1}, 1600 cm^{-1}, 1370 cm^{-1}. HRMS (APCI) *m/z*: [M+H]+ calc'd for ($C_{23}H_{19}ClFN_2O^+$) calc'd for ($C_{23}H_{19}F_2N_2O^+$) 377.1460; Found 377.1408.

N,N-bis(4-fluorophenyl)-2-(1H-indol-1-yl)acetamide (8)

General procedure A produced a white waxy solid (60%). ^{1}H NMR (DMSO-d_6, 500 MHz) δ 7.74 (s, 2H), 7.51 (dt, J = 7.8, 1.0 Hz, 1H), 7.39-7.29 (m, 5H), 7.22 (d, J = 3.2 Hz, 3H), 7.12-7.09 (m, 1H), 7.01-6.98 (m, 1H), 6.39 (dd, J = 3.2, 0.9 Hz, 1H), 4.88 (s, 2H).^{13}C{^{1}H} NMR ($CDCl_3$, 126 MHz) δ 167.8, 138.0, 137.2, 136.2, 129.9, 128.6, 128.3, 127.5, 121.9, 121.1, 119.8, 117.3, 115.9, 108.8, 102.4, 49.5. IR: 3047 cm^{-1}, 2960 cm^{-1}, 1630 cm^{-1}, 1395 cm^{-1}.

HRMS (APCI) *m/z*: [M+H]+ calc'd for ($C_{22}H_{17}ClF_2N_2O^+$) 363.1303; Found 363.1177. *^{1}H NMR and $^{13}C\{^1H\}$ NMR were run in different solvents for better resolution of the observed peaks.

3-(6-chloro-1H-indol-1-yl)-N,N-bis(4-fluorophenyl)propanamide (9)

General procedure A produced a waxy light-brown solid (62%). ^{1}H NMR (DMSO-d_6, 500 MHz) δ 7.54 (d, *J* = 8.4 Hz, 1H), 7.42-7.40 (m, 1H), 7.33 (d, *J* = 3.1 Hz, 1H), 7.21-7.11 (m, 8H), 7.02 (dd, *J* = 8.4, 1.9 Hz, 1H), 6.44 (dd, *J* = 3.2, 0.9 Hz, 1H), 4.41 (t, *J* = 6.7 Hz, 2H), 2.62 (t, *J* = 6.7 Hz, 2H). $^{13}C\{^1H\}$ NMR ($CDCl_3$, 126 MHz) δ 170.7, 138.0, 137.9, 136.0, 129.9 (d, *J* = 8.3 Hz), 129.5, 128.0 (d, *J* = 8.2 Hz), 127.7, 127.3, 121.9, 120.3, 116.8 (d, *J* = 22.9 Hz), 116.0 (d, *J* = 22.5 Hz), 109.3, 101.6, 43.2, 34.9. IR: 3062 cm^{-1}, 2941 cm^{-1}, 1661 cm^{-1}, 1306cm^{-1}. HRMS (APCI) *m/z*: [M+H]+ calc'd for ($C_{23}H_{18}ClF_2N_2O^+$) 411.1070; Found 411.1092. *^{1}H NMR and $^{13}C\{^1H\}$ NMR were run in different solvents for better resolution of the observed peaks.

2-(6-chloro-1H-indol-1-yl)-N,N-bis(4-fluorophenyl)acetamide (10)

General procedure A produced a white solid (77%). MP: 144-145°*C*. ^{1}H NMR (CD_2Cl_2, 500 MHz) δ 7.55 (d, *J* = 8.4 Hz, 1H), 7.38-7.22 (m, 6H), 7.18 (dt, *J* = 1.5, 0.7 Hz, 1H), 7.10 (dd, *J* = 8.4, 1.9 Hz, 2H), 7.02 (d, *J* = 3.3 Hz, 2H), 6.52 (dd, *J* = 3.2, 0.9 Hz, 1H), 4.77 (s, 2H). $^{13}C\{^1H\}$ NMR (CD_2Cl_2, 126 MHz) δ 167.3, 138.5, 137.5, 137.2, 130.7 (d, *J* = 8.2 Hz), 129.9, 128.04, 128.01, 127.5, 122.2, 120.6, 117.9 (d, *J* = 23.9 Hz), 116.2 (d, *J* = 22.9 Hz), 109.4, 102.6, 49.6. IR: 3056 cm^{-1}, 2979 cm^{-1}, 1669 cm^{-1}, 1499 cm^{-1}. HRMS (APCI) *m/z*: [M+H]+ calc'd for ($C_{22}H_{16}F_2ClN_2O^+$) 397.0914; Found 397.0916.

3-(2,3-dihydro-4H-benzo[b][1,4]oxazin-4-yl)-N,N-bis(4-fluorophenyl)propenamide (11)

General procedure B produced a brown waxy solid (47%). ^{1}H NMR ($CDCl_3$, 500 MHz) δ 7.20-7.17 (m, 4H), 7.06-7.03 (m, 4H), 6.82-6.77 (m, 2H), 6.71-6.69 (m, 1H), 6.57 (d, *J* = 8.0 Hz, 1H), 4.25-4.23 (m, 2H), 3.68 (t, *J* = 6.5 Hz, 2H), 3.38-3.36 (m, 2H), 2.61 (t, *J* = 6.5 Hz, 2H). $^{13}C\{^1H\}$ NMR ($CDCl_3$, 126 MHz) δ 171.7, 144.2, 138.4, 134.0, 130.2, 128.0, 121.7, 118.1, 117.1 (d, *J* = 23.0 Hz), 116.5, 116.0. (d, *J* = 22.4 Hz), 112.2, 64.4, 47.72, 47.68, 31.8. (*Missing Ar-Carbon around 140 ppm) IR: 3053 cm^{-1}, 2994 cm^{-1}, 1655 cm^{-1}, 1349 cm^{-1}. HRMS (APCI) *m/z*: [M+H]+ calc'd for ($C_{23}H_{21}F_2N_2O_2^+$) 395.1566; Found 395.1771.

2-(2,3-dihydro-4H-benzo[b][1,4]oxazin-4-yl)-N,N-bis(4-fluorophenyl)acetamide (12)

General procedure B produced a brown waxy solid (70%). ^{1}H NMR (DMSO-d_6, 500 MHz) δ 7.68 (s, 2H), 7.33-7.18 (m, 6H), 6.75-6.72 (m, 1H), 6.64 (dd, *J* = 7.8, 1.5 Hz, 1H), 6.52-6.48 (m, 2H), 4.09-4.07 (m, 2H), 3.93 (s, 2H), 3.36-3.33 (m, 2H). $^{13}C\{^1H\}$ NMR (DMSO-d_6, 126 MHz) δ 169.1, 143.9, 135.4, 134.1, 131.3, 130.2, 129.0, 121.7, 117.5, 117.2, 116.1, 115.8, 111.8, 64.5, 53.0, 47.8. IR: 3067 cm^{-1}, 2975 cm^{-1}, 1700 cm^{-1}, 1245 cm^{-1}. HRMS (APCI) *m/z*: [M+H]+ calc'd for ($C_{22}H_{19}F_2N_2O_2^+$) 381.1409; Found 381.1440.

N,N-bis(4-fluorophenyl)-3-(2-oxobenzo[d]oxazol-3(2H)-yl)propanamide (13)

To a solution of benzo[d]oxazol-2(3H)-one (1.0 equiv) in CH_3CN (5 mL), K_2CO_3 (1.5 equiv) and **S2** (1.15 equiv) were each added. The reaction mixture was stirred for 24 hours at 80°C under inert N_2 gas. The reaction was then cooled to room temperature and concentrated under reduced pressure. The crude mixture was washed with water (2 x 10 mL) and extracted with DCM (20 mL). The organic layer was dried over Na_2SO_4, filtered, concentrated under reduced pressure, and purified using automated Combiflash chromatography (silica gel, 20-40 microns using a mobile phase of 0%-20% EtOAc in Hexane), yielding a white solid (46%). MP: 141-142°*C* ^{1}H NMR (CD_2Cl_2, 500 MHz) δ 7.25-7.20 (m, 6H), 7.16-7.12 (m, 4H), 7.05 (t, *J* = 8.5 Hz, 2H), 4.15 (t, *J* = 6.7 Hz, 2H), 2.77 (t, *J* = 6.7 Hz, 2H). $^{13}C\{^1H\}$ NMR (CD_2Cl_2, 126 MHz) δ 170.0, 154.2, 142.6, 138.4, 138.2, 131.1, 130.3 (d, *J* = 8.8 Hz), 128.2 (d, *J* = 8.4 Hz), 123.8, 122.3, 117.1 (d, *J* = 22.9 Hz), 115.8 (d, *J* = 22.7 Hz), 109.7, 109.0, 38.6, 33.0. IR: 3069 cm^{-1}, 2926 cm^{-1},1760 cm^{-1}, 1666 cm^{-1}, 1501 cm^{-1}. HRMS (APCI) *m/z*: [M+H]+ calc'd for ($C_{22}H_{17}F_2N_2O_3^+$) 395.1202; Found 392.1208.

N,N-bis(4-fluorophenyl)-2-(2-oxobenzo[d]oxazol-3(2H)-yl)acetamide (14)

The procedure detailed for compound **13** was followed, but the CH_3CN solvent was replaced with DMF, yielding a white solid (84 %). MP: 155-156°*C*. ^{1}H NMR ($CDCl_3$, 500 MHz) δ 7.40 (s, 2H), 7.25-7.15 (m, 6H), 7.13 (td, *J* = 7.8, 1.3 Hz, 1H), 7.00 (t, *J* = 8.2 Hz, 2H), 6.95-6.93 (m, 1H), 4.47 (s, 2H). $^{13}C\{^1H\}$ NMR ($CDCl_3$, 126 MHz) δ 165.3, 154.5, 142.6, 137.6, 136.6, 131.0, 130.3, 127.3, 123.9, 122.8, 117.8 (d, *J* = 23.1 Hz), 116.0 (d, *J* = 22.9 Hz), 110.2, 108.6, 44.6 IR: 3065 cm^{-1}, 2930 cm^{-1}, 1764 cm^{-1}, 1666 cm^{-1}. HRMS (APCI) *m/z*: [M+H]+ calc'd for ($C_{21}H_{15}F_2N_2O_3^+$) 381.1045; Found 381.1070.

N,N-bis(4-fluorophenyl)-3-(3-oxo-2,3-dihydro-4H-benzo[b][1,4]thiazin-4-yl)propanamide (15)

General procedure A produced a fluffy white solid (98%) with THF as the solvent in place of DMF. MP:150-151°*C*. ^{1}H NMR (CD_2Cl_2, 500 MHz) δ 7.40 (dd, *J* = 7.7, 1.6 Hz, 1H), 7.27-7.23 (m, 5H), 7.14-7.04 (m, 6H), 4.33 (t, *J*= 6.8 Hz, 2H), 3.35 (s, 2H), 2.62 (t, *J*= 6.8 Hz, 2H). $^{13}C\{^1H\}$ NMR (CD_2Cl_2, 126 MHz) δ 170.3, 165.0, 139.3, 138.6, 138.5, 130.3, 128.5, 128.2, 127.3, 123.9, 123.4, 117.6, 116.9 (d, *J* = 23.2 Hz), 115.7 (d, *J* = 22.8 Hz), 41.5, 32.8, 31.5. IR: 3067 cm^{-1}, 2966 cm^{-1},1677 cm^{-1}, 1656 cm^{-1}, 1497 cm^{-1}. HRMS (APCI) *m/z*: [M+H]+ calc'd for ($C_{23}H_{19}F_2O_2N_2S^+$) 425.1130; Found 425.1173.

N,N-bis(4-fluorophenyl)-2-(3-oxo-2,3-dihydro-4H-benzo[b][1,4]thiazin-4-yl)acetamide (16)

General procedure A produced a fluffy white solid (80%) with THF as the solvent in place of DMF. MP: 90-92°*C*. ^{1}H NMR (CD_2Cl_2, 500 MHz) δ 7.47 (s, 2H), 7.39 (dd, *J* = 7.7, 1.5 Hz, 1H), 7.28-7.25 (m, 3H), 7.18 (s, 2H), 7.06 (td, *J* = 7.6, 1.2 Hz, 3H), 6.99 (dd, *J* = 8.2, 1.2 Hz, 1H), 4.51 (s, 2H), 3.42 (s, 2H). ^{13}C{^{1}H} NMR (CD_2Cl_2, 126 MHz) δ 167.5, 166.2, 140.2, 138.7, 137.7, 130.9, 128.7, 128.1, 127.7, 124.0, 123.9, 117.8, 117.7 (d, *J*= 23.1 Hz), 116.1 (d, *J*= 21.8 Hz), 49.2, 31.6. IR: 3065 cm^{-1}, 2983 cm^{-1}, 1660 cm^{-1}, 1499 cm^{-1}. HRMS (APCI) *m/z*: [M+H]+ calc'd for ($C_{22}H_{17}F_2O_2N_2S^+$) 411.0973; Found 411.0974.

N,N-bis(4-fluorophenyl)-3-morpholinopropanamide (17)

General procedure B produced a white powder (36%) with the following modifications: 1.1 equiv of TEA and 1.2 equiv of morpholine. MP: 99-101°*C*. ^{1}H NMR (DMSO-d_6, 500 MHz) δ 7.53-7.19 (m, 8H), 3.50 (t, *J* = 4.6 Hz, 4H), 2.53 (t, *J* = 7.3 Hz, 2H), 2.32 (t, *J* = 7.3 Hz, 2H), 2.22 (t, *J* = 4.6 Hz, 4H). ^{13}C{^{1}H} NMR (DMSO-d_6, 126 MHz) 171.5, 139.64, 139.62, 131.3, 129.5, 117.1 (d, *J* = 23.9 Hz), 116.1 (d, *J* = 23.7 Hz), 66.6, 54.6, 53.6, 32.3. IR: 3150 cm^{-1}, 2900 cm^{-1}, 1650 cm^{-1}. HRMS (APCI) *m/z*: [M+H]+ calc'd for ($C_{19}H_{21}F_2N_2O_2^+$) 347.1566; Found 347.1722.

N,N-bis(4-fluorophenyl)-2-morpholinoacetamide (18)

General procedure B produced a white powder (30%) with the following modifications: 3 equiv of TEA and 2 equiv of morpholine. MP: 92-94°*C*. ^{1}H NMR (DMSO-d_6, 500 MHz) δ 7.53-7.22 (m, 8H), 3.48 (t, *J* = 4.6 Hz, 4H), 3.02 (s, 2H), 2.34 (t, *J* = 4.5 Hz, 4H). ^{13}C{^{1}H} NMR ($CDCl_3$, 126 MHz) δ 169.2, 138.12, 138.08, 130.3, 127.8, 116.7, 115.9, 66.8, 60.8, 53.7. IR: 3100 cm^{-1}, 2890 cm^{-1}, 1630 cm^{-1}. HRMS (APCI) *m/z*: [M+H]+ calc'd for ($C_{18}H_{19}F_2N_2O_2^+$) 333.1409; Found 333.1425. *^{1}H NMR and ^{13}C{^{1}H} NMR were run in different solvents for better resolution of the observed peaks.

3-(dimethylamino)-N,N-bis(4-fluorophenyl)propanamide (19)

General procedure C produced a white solid (64%). MP:120-121°*C*. ^{1}H NMR (DMSO-d_6, 500 MHz) δ 7.53 (s, 2H), 7.30-7.19 (m, 6H), 2.47 (t, *J* = 7.9, 2H), 2.28 (t, *J* = 7.8, 2H), 2.01 (s, 6H). ^{13}C{^{1}H}NMR (DMSO-d_6, 126 MHz) δ 171.6, 139.7, 139.6, 131.3, 129.5, 117.2 (d, *J* = 24.3 Hz), 116.1(d, *J* = 24.2 Hz), 55.3, 45.4, 32.9. IR: 3060 cm^{-1}, 2939 cm^{-1}, 1663 cm^{-1}, 1495 cm^{-1}, 1236 cm^{-1}. HRMS (APCI) *m/z*: [M+H]+ calc'd for ($C_{17}H_{19}F_2N_2O^+$) 305.1460; Found 305.1506.

2-(dimethylamino)-N,N-bis(4-fluorophenyl)acetamide (20)

General procedure C produced a white solid (48%). MP: 118-119°*C*. ^{1}H NMR ($CDCl_3$, 500 MHz) δ 7.28-7.25-7.23 (m, 4H), 7.09-7.01 (m, 4H), 3.06 (s, 2H), 2.34 (s, 6H). ^{13}C{^{1}H} NMR (DMSO-d_6, 126 MHz) δ 169.7, 139.5, 139.2, 131.3, 129.5, 116.9, 116.2, 61.0, 45.4. IR: 3062 cm^{-1}, 2942 cm^{-1}, 1665 cm^{-1}, 1232 cm^{-1}. HRMS (APCI) *m/z*: [M+H]+ calc'd for ($C_{16}H_{17}F_2N_2O^+$) 291.1303; Found 291.1347. *^{1}H NMR and ^{13}C{^{1}H} NMR were run in different solvents for better resolution of the observed peaks.

QUANTIFICATION AND STATISTICAL ANALYSIS

All statistical analysis was performed with GraphPad Prism. Statistical significance was determined by one-way ANOVA analysis with n = 3 independent experiments, as indicated in the figure legend. Asterisks for statistical significance are displayed as ns: not significant; *p < 0.1; **p < 0.05; ***p < 0.01.